A Carrier-Based Overmodulation Strategy With Minimum Voltage Distortion for Symmetrical n-Phase Induction Motor Drives

Martín Medina-Sánchez, *Graduate Student Member, IEEE*, Alejandro G. Yepes, *Senior Member, IEEE*, Óscar López, *Senior Member, IEEE*, Ayman Samy Abdel-Khalik, *Senior Member, IEEE*, and Jesús Doval-Gandoy, *Member, IEEE*

***Abstract*—Multiphase machines have significant benefits over their three-phase counterparts. One of them is the possibility of further exploiting the dc-link voltage by injecting non-torque-related voltage harmonics in the xy planes. This allows reaching higher modulation indices in the overmodulation (OVM) region of pulsewidth modulation (PWM) while avoiding torque ripple in motors with negligible space harmonic effects. The most prominent OVM techniques are those based on the instantaneous minimization of the xy voltage. These methods were devised just for five-phase drives and have the drawback that they lack generality. This article overcomes this limitation by proposing an OVM strategy for symmetrical induction motor drives with any odd phase number n. The proposal achieves the minimum voltage distortion, and consequently, it greatly mitigates the xy current distortion. Indeed, it attains the lowest current distortion compared with the existing techniques. It relies on carrier-based PWM in its design and implementation stages, and accordingly, it is much simpler than previous methods. Furthermore, the inverter switching frequency (loss) is substantially reduced. Theoretical assessments are given for drives with odd n between 5 and 11. The experiments are performed with a symmetrical nine-phase induction motor with a single neutral point.**

***Index Terms*—DC-link utilization, minimum harmonic distortion, multiphase drives, overmodulation (OVM), pulsewidth modulation (PWM).**

I. Introduction

MULTIPHASE machines are receiving much attention mainly due to their inherent ability to withstand failures [1], [2]. Moreover, as the phase number increases, the per-phase current rating and torque pulsations tend to decay [2], [3]. These benefits, principally provided by the additional degrees of freedom, have made the n-phase ($n > 3$) machines well suited for high-reliability applications [2]. In particular, motors with symmetrical winding distribution are widespread for many phase numbers [1], and they offer enhanced fault tolerance to open-phase faults [4], which are the most typical [1]. Such degrees of freedom of multiphase motors can be decomposed into several orthogonal subspaces by employing the vector space decomposition [3]. Only one of these subspaces, customarily called the $\alpha\beta$ plane, is responsible for the generation of the electromagnetic torque in motors with sinusoidally distributed windings [3]. The non-torque-producing subspaces correspond to several planes, often called xy planes, and one zero-sequence axis for odd n. The harmonics from to the xy planes, which are absent in three-phase machines, may be exploited to enhance certain features of ac drives without causing torque pulsations [3], [5].

One of the most important aspects of ac drives is the dc-link utilization, which can bring advantages [6], [7], [8], [9] such as wider speed range (for given dc-link voltage) or reduced dc-link voltage and, hence, electromagnetic noise (for given maximum ac voltage). To increase to some extent the dc-link utilization in the linear region of pulsewidth modulation (PWM), non-current-producing zero-sequence voltage harmonics are injected to the reference [10]. Nonetheless, to further exploit the dc link, besides adding zero-sequence harmonics to the voltage reference, low-order current-producing harmonics must be injected as well [5], [9]. Then, the inverter operates in overmodulation (OVM) [11], [12].

The most widespread approach adopted in OVM is based on the injection of just xy voltage [5], [7], [9], [13], [14], [15], [16]. In line with this strategy, early attempts of OVM were performed by employing only the two largest space vectors that are the nearest to the voltage reference [17]. This strategy, originally proposed for five-phase drives, can be straightforwardly extended to higher phase numbers [13], [15]. Recently, equivalent techniques, but with carrier-based implementation, have been proposed [7], [8], [16]. In any case, this leads to significant voltage distortion in the xy planes. Hence, considerable current

Manuscript received 1 March 2023; revised 20 June 2023; accepted 18 August 2023. Date of publication 31 August 2023; date of current version 23 October 2023. This work was supported in part by the Government of Galicia under Grants ED431F 2020/07 and GPC-ED431B 2020/03, in part by the Ministry of Science, Innovation and Universities under the Ramon y Cajal Grant RYC2018-024407-I, and in part by the Spanish State Research Agency under Project PID2022-136908OB-I00/AEI. Recommended for publication by Associate Editor T. Shi. *(Corresponding author: Jesús Doval-Gandoy.)*

Martín Medina-Sánchez, Alejandro G. Yepes, Óscar López, and Jesús Doval-Gandoy are with the Applied Power Electronics Technology Research Group, CINTECX, Universidade de Vigo, 36310 Vigo, Spain (e-mail: martindamian.medina@uvigo.es; agyepes@uvigo.es; olopez@uvigo.gal; jdoval@uvigo.es).

Ayman Samy Abdel-Khalik is with the Department of Electrical Engineering, Faculty of Engineering, Alexandria University, Alexandria 21544, Egypt (e-mail: ayman.abdel-khalik@alexu.edu.eg).

This article has supplementary material provided by the authors and color versions of one or more figures available at https://doi.org/10.1109/TPEL.2023.3308599.

Digital Object Identifier 10.1109/TPEL.2023.3308599

harmonics may arise [6], aggravated by the relatively low xy impedances [3]. Much effort has been devoted to mitigating these troublesome currents. Passive current filters were suggested in [7]. Although these filters increase the xy impedance, their main drawback is that they raise the size and cost. Alternatively, in [6] and [18], the current distortion is reduced by decreasing the xy voltage, while low-order torque-producing $\alpha\beta$ harmonics are injected instead. Nonetheless, detrimental effects due torque ripple may appear [5], [19], e.g., speed oscillations, severe vibrations, acoustic noise, etc. [20]. Other approaches have been devised to alleviate the xy voltage distortion without torque pulsations or passive filters, as discussed in the following.

Many OVM methods with just xy voltage injection have been proposed for five-phase drives. In this regard, there are techniques aimed at decreasing/minimizing the voltage distortion [5], [12], [14], [21] or minimizing the stator copper loss [18]. Although the latter achieves the minimum current distortion, it is more complex, as it requires an exhaustive offline optimization for each modulation index. Relatively simpler, a notable method is the one that minimizes at every instant the xy voltage injected [5], [9], [14]. This approach achieves the minimum voltage distortion (MVD) in OVM [18]. Remarkably, the current distortion is also close to its minimum possible for most modulation indices [18]. In particular, the space-vector method proposed in [5] computes in advance certain matrices to be used online for calculating the optimal dwell times of the space vectors. These matrices are the outcome of a minimization problem that includes two equality and five inequality constraints. The solution to this problem is intricate and complex due to the inequality restrictions [13], [15]. Later, a relatively simpler optimization process to said problem was devised in the space-vector technique from [14], and recently, an equivalent carrier-based strategy has been proposed in [9]. Unfortunately, the methods from [5], [9], and [14] lack generality, as they rely on the specific distribution of space vectors for five-phase drives and on the existence of a single xy plane, which hampers their application to machines having more phase numbers. Accordingly, the manner in which the xy harmonics are synthesized is unsuitable for phase numbers n other than five.

On the other hand, little work has been done to mitigate the xy voltage distortion in OVM for greater n. The method from [12] for odd $n \geq 5$ reduces to some extent the xy harmonics. Another technique for odd $n \geq 7$ was devised in [13]. It adopts the concept of intermediate (virtual) vectors, introduced in [15] for six-phase drives, and the xy voltage is the outcome of a sequential optimization scheme [13], [22]. The optimization scheme from [13] injects mainly the lowest order voltage harmonic for modulation indices at the beginning of the OVM range. For greater modulation indices, higher order harmonics are progressively added. Later, a modified sequential optimization scheme has been devised in [22]. It is based on injecting harmonics in the reverse order to [13], i.e., injecting higher order harmonics first. Nonetheless, the strategy from [22] yields more current distortion than that from [13], especially for low modulation indices in OVM [22]. In general, the sequential optimization scheme of [13] and [22] divides the $\alpha\beta$ plane into several sectors and zones. For each zone, one matrix is computed and then stored in the control platform for determining the duty cycles of the space vectors, analogously to [5]. Concerning harmonic distortion, it has been proven that the technique from [13] yields less than that from [12], at least for $n = 7$. For greater n, the performance of [13] is still uncertain. To sum up, these space-vector methods [12], [13], [22] reduce to some extent the harmonic distortion, but none of them ensures the MVD in OVM.

Most of the existing OVM strategies rely on space-vector PWM [5], [12], [13], [14], [22], which is more complex than carrier-based PWM [8], [9], [16]. The former typically needs computing online square roots and trigonometric functions [17], [23], [24], which are time-consuming tasks [7]. In addition, certain strategies (see, e.g., [5], [13], and [14]) require a thorough modeling of the inverter in the design stage: mapping of the 2^n space vectors in each subspace, division of the $\alpha\beta$ plane into several sectors and zones, choosing the active space vectors involved in each sector and zone as well as their switching patterns, etc. Although this offers a better insight into the inverter operation [2], performing these tasks is laborious, especially as n rises [8], [9]. A further complication lies in the fact that most of the available control platforms do not include dedicated hardware modules for multiphase space-vector PWM, but just for carrier-based PWM [23].

In summary, there is no OVM strategy, either carrier-based or space-vector, for any number of phases n capable of attaining the MVD. Furthermore, although carrier-based methods are simpler than space-vector ones, there is no carrier-based OVM strategy for $n \geq 7$ with low harmonic distortion.

Therefore, this article fills these literature gaps by proposing a carrier-based method that attains the MVD in OVM for symmetrical motor drives with an arbitrary odd n. It ensures the MVD while avoiding torque ripple by minimizing at each instant the xy voltage that is injected to the reference. Besides being suitable for any odd n, the additional salient benefits of the method are as follows.

1) As a result of attaining the MVD, the current distortion is greatly mitigated, especially in motors with negligible space harmonics. Actually, it achieves the lowest current distortion compared with existing techniques.
2) It produces the smallest switching frequency and, thus, alleviates the inverter switching losses. Indeed, as a consequence of reaching the lowest current distortion and switching frequency, the proposal improves the overall drive efficiency as it achieves the smallest stator copper losses and inverter losses.
3) It relies on carrier-based PWM. Conveniently, the commissioning does not require performing tedious tasks that are typical for space-vector methods. Similarly, the online execution is also much simpler.

Although the main contribution of this article is the new technique, a thorough study in terms of voltage and current distortion, switching losses, and computational burden is also given for symmetrical motors with odd n between 5 and 11. This provides valuable information about the overall behavior of the most salient OVM techniques. It is highlighted that the proposal is advantageous in all the studied figures of merit, for any phase number. The experiments are performed with a

symmetrical nine-phase induction motor. A preliminary version of this work was presented in [25] only for nine-phase drives. Nonetheless, the generalization of the method for an arbitrary odd n is presented here, including new significant studies in terms of switching frequency, total losses, torque waveforms, and dynamic response.

The rest of this article is organized as follows. The necessary background is reviewed in Section II. The proposed strategy is explained in Section III, and its performance is assessed in Section IV. The experimental results are discussed in Section V. Finally, Section VI concludes this article.

II. Background

A. Vector Space Decomposition

An array of variables in the n phases (with n being odd)

$$\boldsymbol{u} = [u_{\mathrm{a}} \quad u_{\mathrm{b}} \quad u_{\mathrm{c}} \quad \cdots \quad u_n]^{\mathrm{T}} \tag{1}$$

where u stands for voltages or currents, can be decomposed into $P = (n-1)/2$ planes and one zero-sequence axis [3]. This is possible by multiplying the vector space decomposition matrix $\boldsymbol{T}$ in (2) shown at the bottom of this page, where $\varphi = 2\pi/n$, by the per-phase signal vector, as

$$\boldsymbol{U} = \boldsymbol{T}\boldsymbol{u}. \tag{3}$$

The outcome of the multiplication in (3) is

$$\boldsymbol{U} = [u_\alpha \quad u_\beta \quad u_{x,1} \quad u_{y,1} \quad \ldots \quad u_{x,P-1} \quad u_{y,P-1} \quad u_{\mathrm{zs}}]^{\mathrm{T}} \tag{4}$$

with $U_{\alpha\beta} = u_\alpha + \mathrm{j}u_\beta$ being the space vector of the $\alpha\beta$ plane; the space vectors belonging to the xy planes are from $U_{xy,1} = u_{x,1} + \mathrm{j}u_{y,1}$ up to $U_{xy,P-1} = u_{x,P-1} + \mathrm{j}u_{y,P-1}$; and u_{zs} defines the zero-sequence component. From the model of multiphase motors with sinusoidally distributed windings [3], only the $\alpha\beta$ plane develops torque, whereas the xy planes are decoupled from the rotor and just produce losses. Furthermore, the zero-sequence currents are restricted to zero since the windings are assumed to be star connected. The mapping of the harmonic orders in each subspace by using (2) matches that given in [26] for symmetrical odd-n drives. For instance, for $n = 9$ ($P = 4$), the (u_α, u_β) plane contains the harmonic orders $1, 17, 19, \ldots$; $(u_{x,1}, u_{y,1})$, the orders $7, 11, \ldots$; $(u_{x,2}, y_{y,2})$, the orders $3, 15 \ldots$; $(u_{x,3}, u_{y,3})$, the orders $5, 15, \ldots$; and u_{zs}, the orders $9, 27, \ldots$

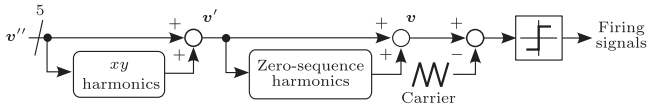

Fig. 1. Scheme of the OVM carrier-based strategy from [9].

B. OVM With MVD for Five-Phase Drives

A review of the OVM methods with MVD just for five-phase drives [5], [9], [14] is given here. Although they lack generality, certain features of them, pointed out here for the first time, are exploited afterward to propose an OVM method with MVD for symmetrical motors with an arbitrary odd phase number in the subsequent section.

The carrier-based method from [9] is considered, which is equivalent to the space-vector ones from [5] and [14]. The scheme from [9] is depicted in Fig. 1. In principle, the reference voltage signals $\boldsymbol{v}''$ are purely sinusoidal and only contain the desired $\alpha\beta$ fundamental component. Then, to attain the latter, the minimum xy voltage is injected, resulting in the signals $\boldsymbol{v}'$. Afterward, the zero-sequence components, which are synthesized by the min–max method [10], are added yielding the modulating signals $\boldsymbol{v}$. Finally, $\boldsymbol{v}$ is compared with the carrier to produce the firing signals. The carrier has a triangular shape whose peak values are ± 1. Thus, the signals $\boldsymbol{v}$ should be within ± 1 p.u. (normalized by one half of the dc-link voltage v_{dc}). The scheme of Fig. 1 is valid for $\boldsymbol{v}''$ in the linear region of PWM if the xy harmonics are set to zero. Determining if $\boldsymbol{v}''$ corresponds to the linear region or to OVM is as simple as calculating the subtraction between its maximum and minimum signals at each instant. If this subtraction is less than or equal to 2 p.u., then $\boldsymbol{v}''$ belongs to the linear region and, otherwise, to OVM. Henceforth, $\boldsymbol{v}''$ in the latter case is simply said to be in OVM.

In the linear region, the addition of just zero-sequence voltage allows reaching a modulation index M up to $M \approx 1.05$ (for $n = 5$) [10], where M is computed as

$$M = \frac{\hat{v}}{0.5 v_{\mathrm{dc}}} \tag{5}$$

with $\hat{v}$ being the fundamental voltage amplitude. If $M > 1.05$ is desired, OVM occurs, where the injection of xy harmonics, as well as zero-sequence ones, is mandatory. In this manner,

$$\boldsymbol{T} = \frac{2}{n}\left[\begin{array}{cccccc}
1 & \cos(\varphi) & \cos(2\varphi) & \cos(3\varphi) & \ldots & \cos((n-1)\varphi) \\
0 & \sin(\varphi) & \sin(2\varphi) & \sin(3\varphi) & \ldots & \sin((n-1)\varphi) \\
1 & \cos(2\varphi) & \cos(2\cdot 2\varphi) & \cos(2\cdot 3\varphi) & \ldots & \cos(2(n-1)\varphi) \\
0 & \sin(2\varphi) & \sin(2\cdot 2\varphi) & \sin(2\cdot 3\varphi) & \ldots & \sin(2(n-1)\varphi) \\
\vdots & \vdots & \vdots & \vdots & \ddots & \vdots \\
1 & \cos(P\varphi) & \cos(P\cdot 2\varphi) & \cos(P\cdot 3\varphi) & \ldots & \cos(P(n-1)\varphi) \\
0 & \sin(P\varphi) & \sin(P\cdot 2\varphi) & \sin(P\cdot 3\varphi) & \ldots & \sin(P(n-1)\varphi) \\
1/2 & 1/2 & 1/2 & 1/2 & \ldots & 1/2
\end{array}\right]\left|\begin{array}{c} u_\alpha \\ u_\beta \\ u_{x,1} \\ u_{y,1} \\ \vdots \\ u_{x,P-1} \\ u_{y,P-1} \\ u_{\mathrm{zs}} \end{array}\right. \tag{2}$$

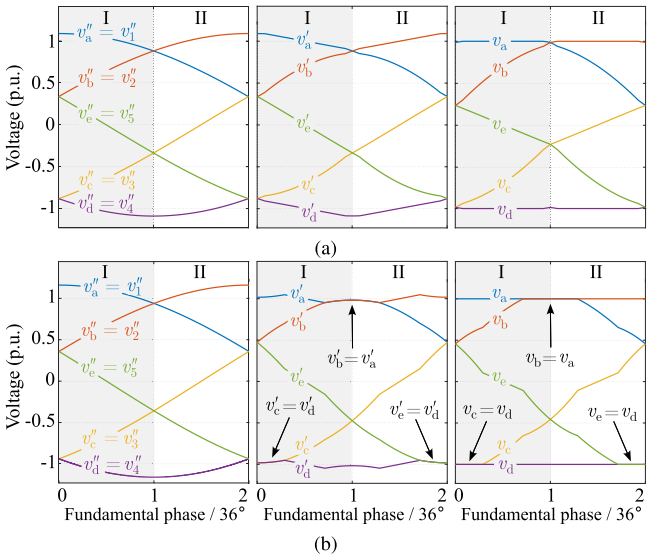

Fig. 2. Pole-voltage waveforms, normalized by $0.5v_{\mathrm{dc}}$, of the method from [9] (just for $n = 5$) for (a) $M = 1.09$ and (b) $M = 1.16$. The phase angle is normalized by $\varphi/2 = 36°$, and the first two of the ten sectors of symmetry in one fundamental period are shown.

M may be raised from 1.05 up to 1.23 without injecting $\alpha\beta$ harmonics [5], [9].

The signals $\boldsymbol{v}''$, $\boldsymbol{v}'$, and $\boldsymbol{v}$ are depicted in Fig. 2 for certain M. For clarity, this figure shows only two of the ten sectors of symmetry in which one fundamental period can be divided for $n = 5$ [7], [23]. Fig. 2(a) depicts the behavior of the method from [9] for a relatively low M, e.g., $M = 1.09$, in the range $1.05 < M \leq 1.10$. For this particular range, the inverter alternatively operates at some phase angles between the OVM and the linear region, depending on whether $\boldsymbol{v}''$ is or not in OVM. For said range, the per-phase components of $\boldsymbol{v}'$ are in general different from each other. As reported in [9], the injection of the minimum xy voltage (for $\boldsymbol{v}''$ in OVM) renders the difference between the highest and the lowest phase signals of $\boldsymbol{v}'$ equal to 2 p.u. at every sample. On the other hand, the behavior of the strategy from [9] for a greater M, e.g., $M = 1.16$, in the range of $1.10 < M \leq 1.23$ is shown in Fig. 2(b). In this range, the inverter operates in OVM for the entire fundamental period. Similarly, the subtraction between the highest and the lowest signals of $\boldsymbol{v}'$ remains equal to 2 p.u. due to the injection of the minimum xy voltage. In addition, several components of $\boldsymbol{v}'$ overlap for certain phase angles. For instance, at the end of the first sector, the highest $\boldsymbol{v}'$ signals (v'_{a} and v'_{b}) match; on the other hand, at the beginning, the lowest ones (v'_{c} and v'_{d}) match. In any case, as can be seen in the illustrations at the right column of Fig. 2, the aforesaid characteristics for $\boldsymbol{v}'$ also hold for $\boldsymbol{v}$. In addition, $\boldsymbol{v}$ also contains the zero-sequence harmonics, which ensure that its highest and lowest pole voltages are located at the same distance from zero at each instant [7]. Hence, for $\boldsymbol{v}''$ in OVM, the highest and lowest components of $\boldsymbol{v}$ are clamped to 1 and -1 p.u., respectively, at every instant.

As aforesaid, the guidelines given in [5], [9], and [14] for synthesizing the xy voltage are unsuitable for $n > 5$. This is overcome by the proposal, hereafter referred to simply as MVD.

III. MVD OVM Method for n Phases

To achieve the desired modulation index in OVM with minimum voltage total harmonic distortion (THD), the proposed method should inject the minimum xy voltage as well as the appropriate zero sequence at each instant. Then, the optimum final pole-voltage references $\boldsymbol{v}$ are obtained. To this end, certain matrices that permit to calculate $\boldsymbol{v}$, as a function of the $\alpha\beta$ components of a given voltage reference $\boldsymbol{v}''$ in OVM, are computed offline and stored. These matrices are the outcome of an optimization problem carried out by using $\boldsymbol{v}''$ in the first sector. To straightforwardly employ these matrices for all other sectors, a procedure for obtaining symmetry with respect to the first one is given in the following.

A. Symmetrical Sectors for Multiphase Drives

To facilitate the analysis and implementation of a carrier-based PWM, one fundamental period can be partitioned into $2n$ sectors spanning $\varphi/2$ [16]. For instance, Fig. 3 shows the first nine sectors for $n = 9$, while the first two sectors for $n = 5$ match those of Fig. 2. In each sector, the order of the phase signals of $\boldsymbol{v}''$ can be conveniently arranged to obtain several identical or symmetrical sectors [7]. In [7], [9], and [16], said signals are sorted at every instant from the highest to the lowest values. Nonetheless, if the transformation from (3) is directly applied to these sorted signals, the resulting $\alpha\beta$ components are neither equal nor symmetrical to those of $\boldsymbol{v}''$ for the first sector. To solve this problem, a two-step sorting procedure is carried out.

In the first step, the phase components of $\boldsymbol{v}''$, given by

$$\boldsymbol{v}'' = \begin{bmatrix} v''_1 & v''_2 & v''_3 & \dots & v''_{P+1} & v''_{n-(P-1)} & \dots & v''_{n-1} & v''_n \end{bmatrix}^{\mathrm{T}} \tag{6}$$

are sorted from highest to lowest, similarly to [7], [9], and [16]. For simplicity, the subscripts identifying phase variables in (6) are replaced by numbers, i.e., $v''_1 = v''_{\mathrm{a}}$, $v''_2 = v''_{\mathrm{b}}$, etc. After sorting $\boldsymbol{v}''$ in decreasing manner, $\bar{\boldsymbol{v}}$ is obtained. Namely, for an n-phase drive, in the first sector

$$\overbrace{\begin{bmatrix} \bar{v}_1 & \bar{v}_2 & \bar{v}_3 & \bar{v}_4 & \bar{v}_5 & \dots & \bar{v}_{n-1} & \bar{v}_n \end{bmatrix}^{\mathrm{T}}}^{\bar{\boldsymbol{v}}} = \begin{bmatrix} v''_1 & v''_2 & v''_n & v''_3 & v''_{n-1} & \dots & v''_{P+1} & v''_{n-(P-1)} \end{bmatrix}^{\mathrm{T}}. \tag{7}$$

The pole voltages located at even positions in the right-hand side of (7) follow the pattern $v''_2, v''_3, \dots, v''_{P+1}$, whereas those in odd positions (disregarding the first one) follow the descending pattern $v''_n, v''_{n-1}, \dots, v''_{n-(P-1)}$. This order can be seen, e.g., in the first sector of Figs. 2 and 3(a) for $n = 5$ ($P = 2$) and $n = 9$ ($P = 4$), respectively. The additional step proposed next rearranges $\bar{\boldsymbol{v}}$ to keep the original phase sequence [that of (6)], yielding $\hat{\boldsymbol{v}}$. From (7), since $\bar{v}_1 = v''_1$, $\bar{v}_2 = v''_2$, $\bar{v}_3 = v''_n$ and so

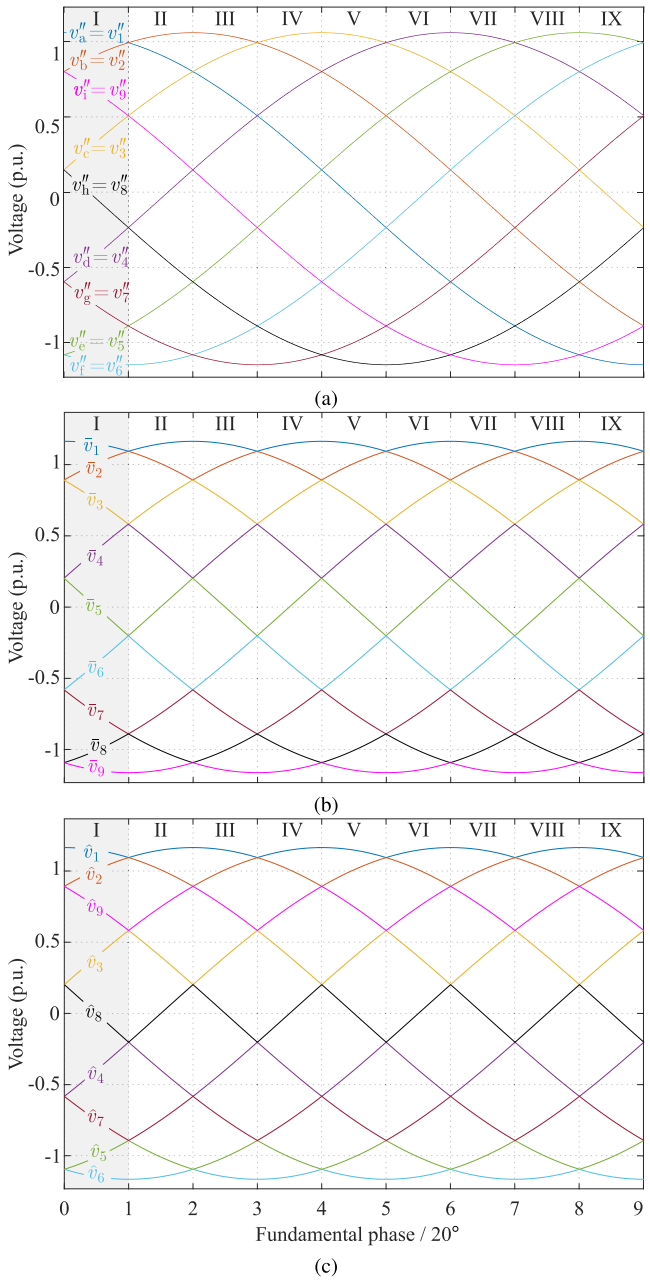

Fig. 3. Pole-voltage waveforms for $M = 1.16$, normalized by $0.5v_{\mathrm{dc}}$, of the MVD method for $n = 9$. The phase angle is normalized by $\varphi/2 = 20°$ and the first nine of the $2n = 18$ sectors of symmetry in one fundamental period are shown. (a) Reference phase signals $\boldsymbol{v}''$. (b) Signals sorted in decreasing order $\bar{\boldsymbol{v}}$. (c) Result of the two-step sorting procedure $\hat{\boldsymbol{v}}$.

on, $\hat{\boldsymbol{v}}$ for the first sector is

$$\overbrace{\begin{bmatrix}\hat{v}_1 & \hat{v}_2 & \hat{v}_3 & \dots & \hat{v}_{P+1} & \hat{v}_{n-(P-1)} & \dots & \hat{v}_{n-1} & \hat{v}_n\end{bmatrix}}^{\hat{\boldsymbol{v}}}{}^{\mathrm{T}} = \begin{bmatrix}\bar{v}_1 & \bar{v}_2 & \bar{v}_4 & \dots & \bar{v}_{n-1} & \bar{v}_n & \dots & \bar{v}_5 & \bar{v}_3\end{bmatrix}^{\mathrm{T}}. \tag{8}$$

This two-step sorting is carried out at each instant maintaining the indices given in (8), not only for the first sector, but for all sectors. As can be seen in Fig. 3(c), the phase order of $\hat{\boldsymbol{v}}$

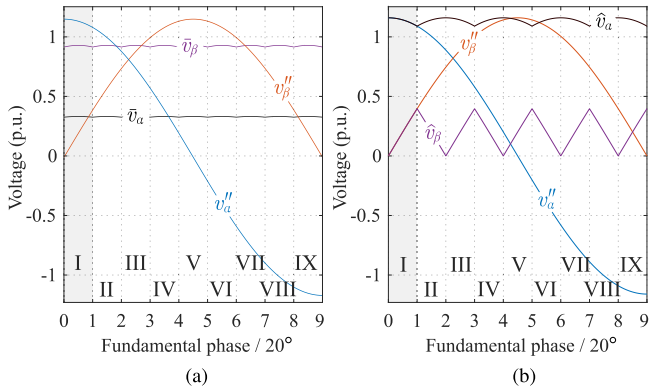

Fig. 4. $\alpha\beta$ voltage waveforms for $M = 1.16$, normalized by $0.5v_{\mathrm{dc}}$, of the MVD method for $n = 9$ for the first nine sectors of symmetry. The $\alpha\beta$ components of $\boldsymbol{v}''$ are compared with those of (a) $\bar{\boldsymbol{v}}$ and (b) $\hat{\boldsymbol{v}}$.

along one fundamental period matches that of $\boldsymbol{v}''$ for the first sector [see Fig. 3(a)]. The $\alpha\beta$ waveforms [after applying (3)] of $\boldsymbol{v}''$ are compared with those of $\bar{\boldsymbol{v}}$ and $\hat{\boldsymbol{v}}$ in Fig. 4, also for $n = 9$. As aforesaid, the $(\bar{v}_\alpha, \bar{v}_\beta)$ voltages are neither equal nor symmetrical to those of the reference (v''_α, v''_β) for the first sector [see Fig. 4(a)]. This condition is corrected by $(\hat{v}_\alpha, \hat{v}_\beta)$ in Fig. 4(b). As can be seen, $(\hat{v}_\alpha, \hat{v}_\beta)$ in odd sectors are identical to (v''_α, v''_β) for the first sector. For even sectors, $(\hat{v}_\alpha, \hat{v}_\beta)$ are symmetrical to (v''_α, v''_β) for the first sector. Broadly speaking, this two-step sorting procedure is analogous to that used in the space-vector methods for rotating the $\alpha\beta$ vector to the first sector [17], [23], [24], but without sector identification, square roots, or trigonometric functions. As aforesaid, this advantage is of considerable importance, taking into account that these tasks are regarded as time consuming [23].

By taking advantage of the symmetry provided by the two-step sorting, the optimization problem is put forward next only for the first sector, and its solution is then straightforwardly employed for the entire fundamental period.

B. Offline Optimization Problem

For a given voltage reference $\boldsymbol{v}''$ in OVM, MVD computes at every instant the optimum pole voltages $\boldsymbol{v}$ that minimize the xy components injected to the reference. These harmonics are minimized by reducing as much as possible the summation of the squared magnitudes of all the xy space vectors. Hence, the cost function to be minimized is

$$J = \sum_{k=3}^{n-1} \left(\sum_{l=1}^{n} T_{k,l} v_l \right)^2 \tag{9}$$

where $T_{k,l}$ is the element in the kth row and the lth column of $\boldsymbol{T}$. On the other hand, v_l are the pole voltages of $\boldsymbol{v}$, which are considered as variables to be computed. In addition, the optimization problem incorporates some equality constraints. Namely, the $\alpha\beta$ components of $\boldsymbol{v}$ must match those of $\boldsymbol{v}''$ in the first sector. Furthermore, extrapolating the optimum $n = 5$ behavior from Fig. 2(a) to higher n, it follows that, for a relatively low M, the highest phase signal in $\boldsymbol{v}$ and the lowest one should equal 1 and -1 p.u., respectively. For determining which signals

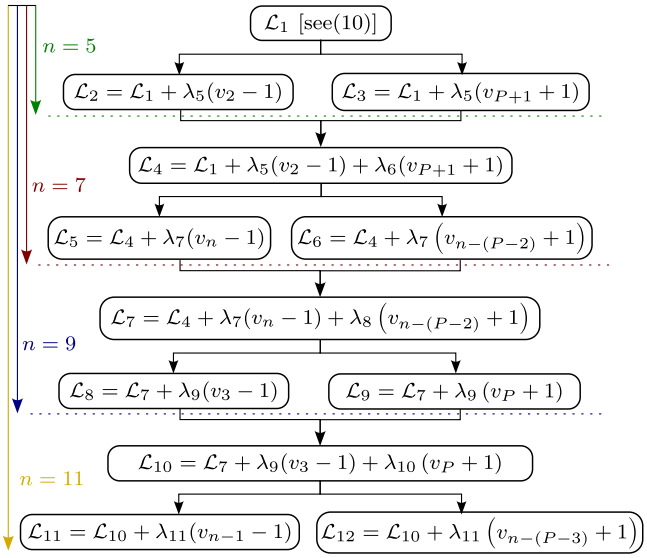

Fig. 5. Scheme of the Lagrangian functions $\mathcal{L}_p$ for the offline optimization of the MVD method for drives with $n=5,7,9,11$.

are these, it can be considered that the phase order (from 1 to n) of $\boldsymbol{v}$ should equal to that of $\boldsymbol{v}''$ for the first sector (see Fig. 2). In this regard, (7) shows the elements of $\boldsymbol{v}''$ arranged in order of decreasing value for the first sector, which must correspond to that of $\boldsymbol{v}$ also sorted in decreasing order. Hence, the signal that reaches 1 p.u. is v_1, which corresponds to the largest component of $\boldsymbol{v}$. Analogously, but for the lowest phase signal, the one that reaches -1 p.u. is $v_{n-(P-1)}$. For instance, this signal matches $v_4=v_\mathrm{d}$ in the first sector of Fig. 2(a).

Using the method of Lagrange multipliers [27], the Lagrangian function including J and these constraints is

$$\mathcal{L}_1=J+\lambda_1\left(\sum_{l=1}^{n}T_{1,l}v_l-\ v''_\alpha\right)+\lambda_2\left(\sum_{l=1}^{n}T_{2,l}v_l-\ v''_\beta\right)+\lambda_3(v_1-1)+\lambda_4\left(v_{n-(P-1)}+1\right) \tag{10}$$

with λ denoting the Lagrange multipliers. By calculating the partial derivatives of (10) with respect to v_l (for $l=1,\ldots,n$) and to the Lagrange multipliers λ_m (for $m=1,\ldots,4$) and then equating them to zero, a system is obtained. After solving this system for $\boldsymbol{v}$, it results in a function of (v''_α,v''_β) as

$$\boldsymbol{v}=\boldsymbol{G_1}\begin{bmatrix}v''_\alpha & v''_\beta\end{bmatrix}^\mathrm{T}+\boldsymbol{C_1} \tag{11}$$

where $\boldsymbol{G_1}\in\mathbb{R}^{n\times 2}$ and $\boldsymbol{C_1}\in\mathbb{R}^{n\times 1}$ are constants.

The solution of the optimization problem listed so far is suitable for relatively low M in OVM (e.g., $M\leq 1.10$ for $n=5$). For greater M, some other phases of $\boldsymbol{v}$ must also equal 1 and -1 p.u., as shown in Fig. 2(b). Therefore, as M increases, more equality constraints are incorporated into (10), giving rise to the Lagrangian functions $\mathcal{L}_p$ (for $p=1,\ldots,3(P-1)$) needed. Fig. 5 summarizes the process to obtain $\mathcal{L}_p$ for $n=5,7,9,11$. The scheme in Fig. 5 is systematic in the sense that the restrictions are progressively added as n grows. For example, $\mathcal{L}_2$ also includes the constraint for $v_2=1$ p.u., which corresponds to the second largest signal [see (7)]. Similarly, $\mathcal{L}_3$ includes the restriction for $v_{P+1}=-1$ p.u., which is the second (from lowest to highest) smallest signal. For instance, in the first sector for $n=5$ and $1.10<M\leq 1.23$ [see Fig. 2(b)], $\mathcal{L}_2$ should also incorporate the restriction for $v_2=v_\mathrm{b}=1$ p.u., and similarly, $\mathcal{L}_3$, also the constraint for $v_3=v_\mathrm{c}=-1$ p.u. Subsequently (if $n>5$), $\mathcal{L}_4$ incorporates both constraints simultaneously, and so on. The approach outlined here is also valid for higher n. Solving an optimization problem that includes equality restrictions is a mechanical task. Indeed, the process for determining the pairs $\boldsymbol{G}_p\in\mathbb{R}^{n\times 2}$ and $\boldsymbol{C}_p\in\mathbb{R}^{n\times 1}$ for the corresponding $\mathcal{L}_p$ functions is the same as that explained for computing $\boldsymbol{G}_1$ and $\boldsymbol{C}_1$ based on (10) and (11).

A maximum number of $3(P-1)$ values of $\boldsymbol{G}_p$ and $\boldsymbol{C}_p$ are needed to compute the optimum elements of $\boldsymbol{v}$. For instance, just three values of $\boldsymbol{G}_p$ and $\boldsymbol{C}_p$ are required for $n=5$:

$$\boldsymbol{G}_1=\begin{bmatrix}0 & a_1 & a_2 & 0 & a_3\\ 0 & a_4 & a_5 & 0 & a_6\end{bmatrix}^\mathrm{T},\quad \boldsymbol{C}_1=\begin{bmatrix}1 & a_7 & -a_7 & -1 & 0\end{bmatrix}^\mathrm{T}$$

$$\boldsymbol{G}_2=\begin{bmatrix}0 & 0 & a_8 & 0 & a_9\\ 0 & 0 & a_{10} & 0 & a_{11}\end{bmatrix}^\mathrm{T},\quad \boldsymbol{C}_2=\begin{bmatrix}1 & 1 & -a_{12} & -1 & -a_{12}\end{bmatrix}^\mathrm{T}$$

$$\boldsymbol{G}_3=\begin{bmatrix}0 & -a_8 & 0 & 0 & -a_8\\ 0 & -a_{10} & 0 & 0 & a_{10}\end{bmatrix}^\mathrm{T},\quad \boldsymbol{C}_3=\begin{bmatrix}1 & a_{12} & -1 & -1 & a_{12}\end{bmatrix}^\mathrm{T}. \tag{12}$$

The values of the a constants in (12) are detailed in the Appendix. Note that, for a given n, $\boldsymbol{G}_p$ and $\boldsymbol{C}_p$ are constant and do not depend on the ratings, parameters, or loading condition of the motor. $\boldsymbol{G}_p$ and $\boldsymbol{C}_p$ for $n=7,9,11$ are included in the supplementary material, so it is not necessary to repeat the offline optimization procedure again. During commissioning, $\boldsymbol{G}_p$ and $\boldsymbol{C}_p$ are stored in the control platform.

C. Online Implementation

Using the stored $\boldsymbol{G}_p$ and $\boldsymbol{C}_p$ matrices found offline, MVD computes online at each instant the optimum $\boldsymbol{v}$ for a reference voltage $\boldsymbol{v}''$ in OVM. First, the two-step sorting is performed. Subsequently, $\boldsymbol{v}$ is calculated similarly to (11), but using instead the $\alpha\beta$ components of $\hat{\boldsymbol{v}}$, as

$$\boldsymbol{v}=\boldsymbol{G}\begin{bmatrix}\hat{v}_\alpha & \hat{v}_\beta\end{bmatrix}^\mathrm{T}+\boldsymbol{C} \tag{13}$$

where $\boldsymbol{G}$ and $\boldsymbol{C}$ equal $\boldsymbol{G}_p$ and $\boldsymbol{C}_p$ corresponding to a certain p. Instead of determining beforehand for which M and phase angle each pair $\boldsymbol{G}_p$ and $\boldsymbol{C}_p$ is suitable, MVD adopts a simple iterative approach, shown in Fig. 6. In this figure, the same n values as in Fig. 5 are considered. Note that $\boldsymbol{v}$ is computed by (13) after each assignment of $\boldsymbol{G}$ and $\boldsymbol{C}$ shown in Fig. 6. The logic behind the iterative scheme is as follows. The $\boldsymbol{G}_1$ and $\boldsymbol{C}_1$ pair is used for the first iteration to compute $\boldsymbol{v}$. Afterward, it is checked if each element of $\boldsymbol{v}$ is between 1 and -1 p.u. To this end, it is enough to check if the phase signals of $\boldsymbol{v}$ that are the closest to 1 p.u. (v_2) and -1 p.u. (v_{P+1}) comply with these limits. If this condition is satisfied, the algorithm has found the optimal values of $\boldsymbol{v}$ and then finishes the iterative process. Otherwise, the remaining $\boldsymbol{G}_p$ and $\boldsymbol{C}_p$ pairs are used in the subsequent iterations until the optimal $\boldsymbol{v}$ is found. In Fig. 6, the sequence in which $\boldsymbol{G}_p$

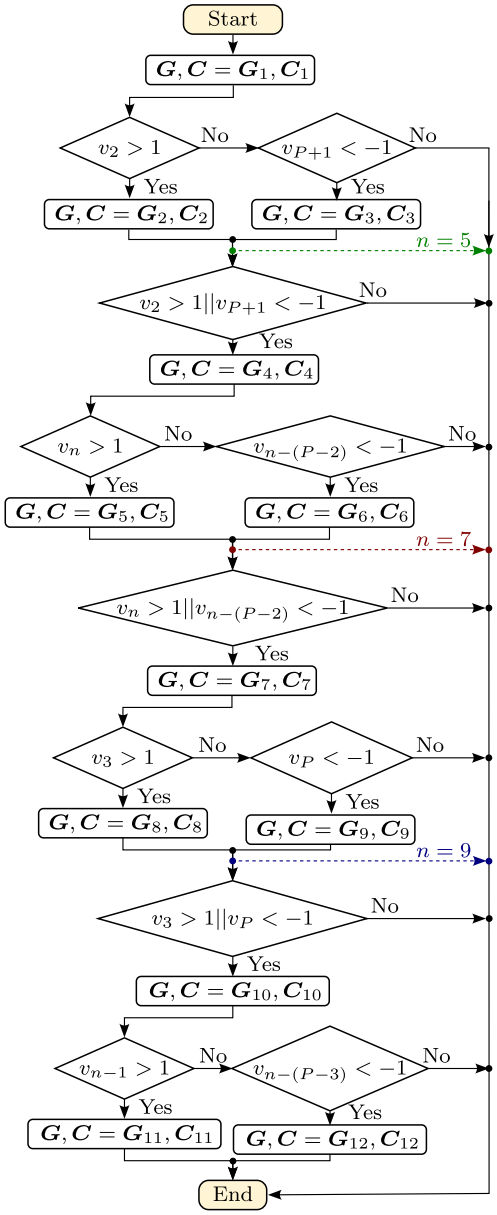

Fig. 6. Flowchart for determining $\boldsymbol{v}$ online using (13) for drives with $n = 5, 7, 9, 11$. The symbol || stands for logical OR operation.

and $\boldsymbol{C}_p$ are used is analogous to that of Fig. 5 for incorporating the equality constraints.

The scheme in Fig. 6 yields an acceptable number of iterations. In the worst case, i.e., when the maximum number of iterations is reached, $n-3$ iterations are carried out. In each iteration, only $2n$ multiplications and $2n$ additions are needed by using (13). Computing such number of multiplications/additions is almost trivial for available control platforms [16], [28]. In fact, since many of the elements of $\boldsymbol{G}_p$ are zero, several multiplications/additions can be omitted. For example, for $n = 5$ in (12), various elements of $\boldsymbol{G}_1$ are zero, as well as most of $\boldsymbol{G}_2$ and $\boldsymbol{G}_3$.

The online implementation of MVD is summarized in Fig. 7. For $\boldsymbol{v}''$ in OVM, MVD performs the two-step sorting in the initial stage. Then, the $\alpha\beta$ components of $\hat{\boldsymbol{v}}$ are used to compute $\boldsymbol{v}$ by applying Fig. 6. Finally, to obtain the firing signals, $\boldsymbol{v}$ is

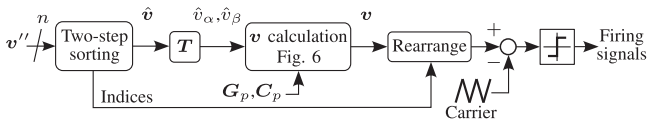

Fig. 7. Overview of the online implementation of MVD for $\boldsymbol{v}''$ in OVM.

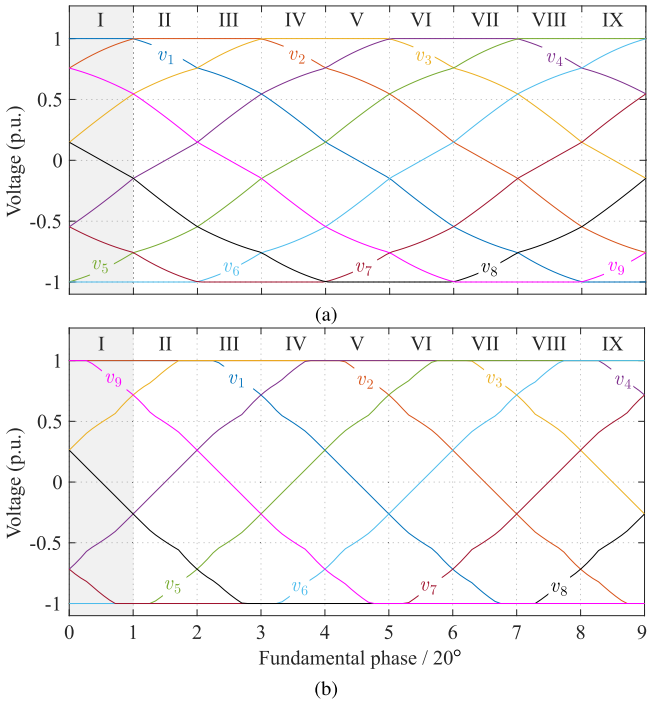

Fig. 8. Final pole-voltage waveforms $\boldsymbol{v}$ for (a) $M = 1.03$ and (b) $M = 1.16$, normalized by $0.5v_{\mathrm{dc}}$, of the MVD method for $n = 9$. The phase angle is normalized by $\varphi/2 = 20°$, and the first nine sectors of symmetry in one fundamental period are shown.

rearranged before the comparison with the carrier. This rearrangement, which is analogous to that used in [6], [7], and [16], is carried out by using the indices employed to sort $\boldsymbol{v}''$. If $\boldsymbol{v}''$ is not in OVM, just min–max zero-sequence voltage is injected, as in the conventional methods.

Fig. 8 shows the final waveforms $\boldsymbol{v}$ of MVD for two M in OVM for $n = 9$. For $M = 1.03$ [see Fig. 8(a)], only two signals equal 1 and -1 p.u. at any instant. For example, for the first sector, said signals are v_1 (1 p.u.) and v_6 (-1 p.u.), which comply with the constraints in $\mathcal{L}_1$ [see (10)]. For $M = 1.16$ (as in Fig. 3), $\boldsymbol{v}$ is depicted in Fig. 8(b). As can be seen, other waveforms of $\boldsymbol{v}$ also achieve these limits at some phase angles, e.g., at the beginning of the first sector, v_1, v_2, and v_9 reach 1 p.u., while v_5 and v_6 reach -1 p.u. This behavior is consistent with the restrictions imposed by $\mathcal{L}_5$ (see Fig. 5).

Note that MVD injects to the reference the minimum xy voltages and the appropriate zero-sequence harmonics as well. The latter is mainly because of the fact that the resulting signals $\boldsymbol{v}$ are already centered between 1 and -1 p.u. (see Fig. 8). Therefore, MVD does not need any additional approach to synthesize the zero-sequence harmonics for a given $\boldsymbol{v}''$ in OVM, as it is the case for most of the existing OVM techniques that rely on carrier-based PWM [6], [7], [9].

TABLE I
MAIN FEATURES OF THE EXISTING METHODS AND THE PROPOSED MVD AND RESULTS OF THE PERFORMANCE ASSESSMENTS

Method	Ref.†	Method description	PWM	n	Minimum voltage THD	Current THD	Average switching frequency	Computational burden
CB	[9]	Minimization of instantaneous xy voltage	Carrier-based	5	Yes	Low	Low	Low
SV1	[5], [14]	Minimization of instantaneous xy voltage	Space-vector	5	Yes	Low	Low	High
SV2	[12]	Reduction of xy voltage to some extent	Space-vector	Any‡	No	High	High	Medium
SV3	[13]	Sequential optimization scheme	Space-vector	≥ 7‡	No⋆	Medium	Medium	High
Proposed MVD		Minimization of instantaneous xy voltage	Carrier-based	Any‡	Yes	Low	Low	Very low

† Ref. stands for Reference. ‡Suitable for odd n. ⋆Reaches the minimum voltage THD just for extremely high modulation indices.

The features of MVD are in agreement with those exposed in Section III-B, which have been extrapolated from $n = 5$ (see Fig. 2) to any odd n for the first time. Furthermore, it has been verified beforehand that MVD achieves the global minimum voltage THD for any M and odd n. This verification was carried out by comparing for $n = 5, 7, 9, 11$ the instantaneous optimum values of $\boldsymbol{v}$, as well as the voltage THD of the proposal, with those produced by solving an optimization problem, different from the one in Section III-B. The main difference is that, besides the restriction related to the $\alpha\beta$ components, no other equality constraints are considered. Instead, just inequality restrictions are imposed for each element of $\boldsymbol{v}$: -1 p.u. $\leq v_l \leq 1$ p.u. These conditions provide an optimization problem with less restrictive constraints to ensure that the global optimum values of $\boldsymbol{v}$ are found. This problem was solved with the command *fmincon* of MATLAB. Although this optimization problem attains the minimum voltage THD, as the proposed method, it is time consuming due to inequality restrictions; thus, it is unsuitable for online execution.

MATLAB/Simulink models of the MVD method for $n = 5, 7, 9, 11$ are included as supplementary material of this article.

IV. PERFORMANCE COMPARISONS

In the following, the performance of the proposed MVD scheme is assessed by numerical simulations. The OVM methods from [5], [9], [12], [13], and [14] are also considered. For $n = 5$, the space-vector methods from [5] and [14] are labeled SV1, while the carrier-based strategy from [9] is called CB. For higher n, the space-vector approaches from [12] and [13] are denoted SV2 and SV3, respectively. Certain important features of these techniques, including the proposed MVD, are given in Table I. A summary of the results, discussed shortly, is included in Table I as well. The methods that rely on the use of only two large space vectors [17] and their carrier-based equivalents [7], [8], [16] are disregarded in this study, since it is well known that they produce much more current distortion [12], [13], [15].

The voltage THD, the current THD, the inverter average switching frequency, and the computational burden are taken into account. The current THD is estimated through the voltage weighted THD (WTHD) [5], [19]. Windings with negligible space harmonics are assumed [2]. Moreover, it is considered that the windings are star connected with a single isolated neutral point. Although MVD is also valid for several neutral points, setting a single one enables enhanced fault tolerance [4], especially for open-phase faults, which are the most common type [1]. A typical sampling frequency of 10 kHz is set [13], [14], [18], and current-producing voltage harmonics are used to compute the voltage THD and voltage WTHD [5], [18], [19]. Since in OVM the most significant current distortion is caused by low-order voltage harmonics [13], [15], [21], higher order ones due to inverter switching are neglected. Furthermore, the frequency of the triangle carrier is 10 kHz, while the fundamental voltage frequency is set to 50 Hz. To generate the inverter firing signals for MVD, the symmetrical regular-sampled carrier-based PWM is employed [29], where each reference sample is taken at the negative peak of the carrier. In this regard, a particular example of a switching sequence for $n = 5$ when using symmetrical regular-sampled PWM can be seen, e.g., in [23, Fig. 7]. Nevertheless, note that the particular technique for generating the firing signals does not significantly influence the low-order harmonics [29]. To provide sufficient insight into the performance of MVD, symmetrical machines with $n = 5, 7, 9, 11$ are considered.

A. Analysis of Harmonic Distortion

The voltage THD and the estimation of the current THD, versus the modulation index M, are shown at the left and right columns of Fig. 9, respectively. The M values span the entire OVM range available by injecting xy harmonics [12].

As shown in Fig. 9, SV2 produces considerable voltage and current distortion regardless of M and n. For $n = 5$ in Fig. 9(a), the voltage and current THDs of the proposed MVD are identical to those of SV1 and CB. Thus, the proposal is fully equivalent to SV1 and CB (only for $n = 5$) in terms of THD. Most importantly, the current THDs are the smallest for the entire OVM range. Reducing the current THD is desirable as it mitigates the harmonic stator copper losses [16], [18], [30] and the inverter conduction losses [18], [31].

For odd $n > 5$, for which SV1 and CB are inappropriate, the proposal also provides the minimum voltage THDs and the lowest current THDs. This fact is depicted in Fig. 9(b)–(d), where MVD notably mitigates the THDs, particularly for relatively low M. Concerning SV3, which is unsuitable for $n = 5$, it reaches the reduced THD of MVD only for a small M range. This corresponds to extremely high M, where significant current harmonics are almost unavoidable. In fact, these large currents may compromise the integrity of the drive [6]. Hence, high M is not advisable, especially for prolonged periods [16].

Furthermore, the advantage of the proposed MVD over SV2 and SV3 becomes more significant as n rises. This can be seen

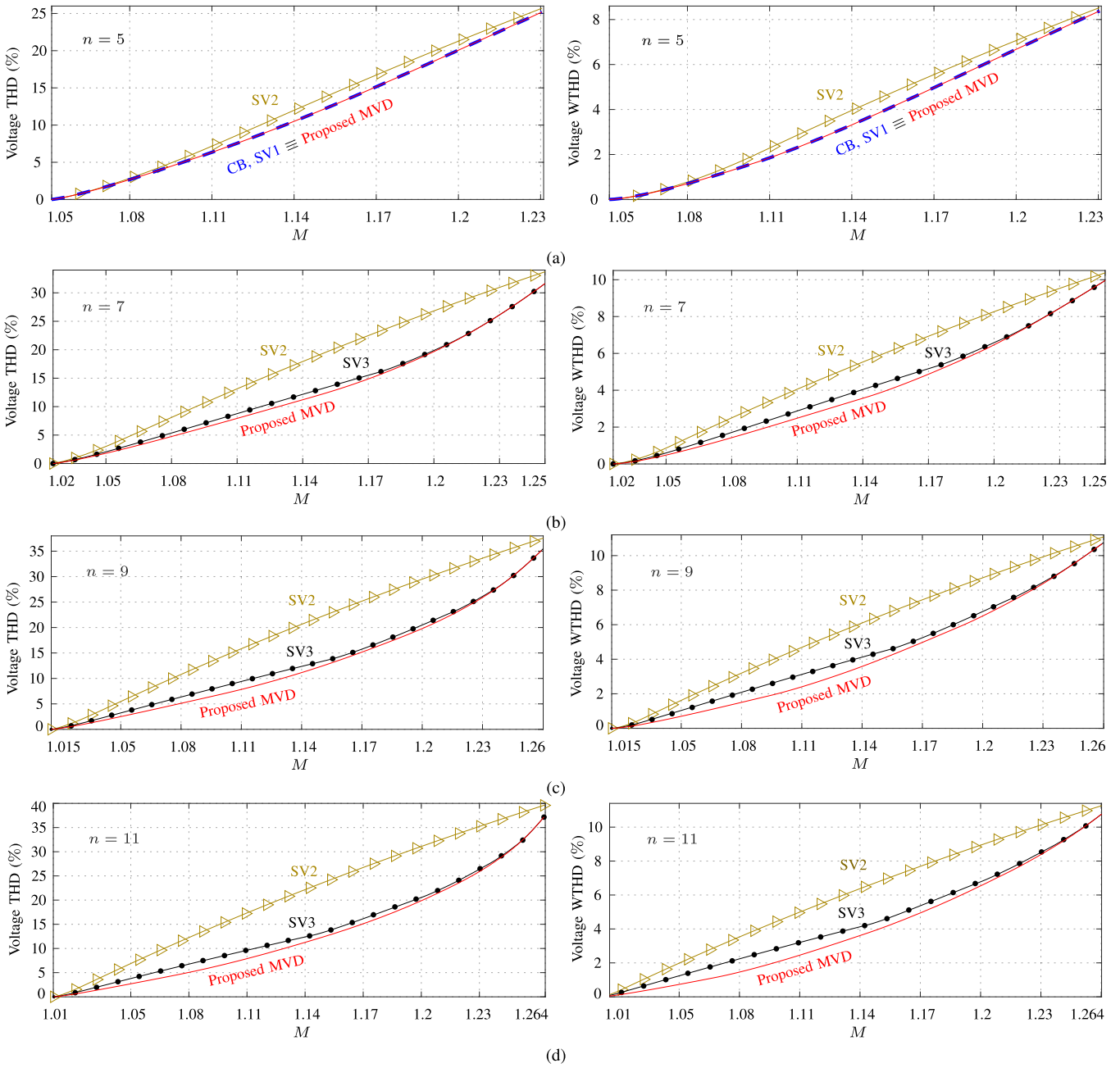

Fig. 9. Comparison of voltage THD and voltage WTHD (current THD) versus M in OVM for (a) $n = 5$, (b) $n = 7$, (c) $n = 9$, and (d) $n = 11$.

in Fig. 9(c) and (d) for $n = 9$ and $n = 11$. The maximum (per n) drop of THD by using the proposal instead of the existing methods is shown in Fig. 10. For $n = 11$, the greatest reduction (simple subtraction) of voltage THD by employing the proposal is 1.82% (SV3) or 11.6% (SV2). Also, for $n = 11$, the maximum reduction of current THD is 0.8% (SV3) or 2.8% (SV2). The significant reduction of 0.8% with respect to SV3 occurs for $M \approx 1.09$ in Fig. 9(d), where the current THD is lowered from 2.57% (SV3) to 1.77%.

Therefore, as summarized in Table I, the proposed MVD reaches the minimum voltage THD for every M and any odd n. As a result, the current THD is notably mitigated.

B. *Analysis of Average Switching Frequency*

The inverter switching losses are proportional to the average switching frequency [9], [32]. Lowering the switching frequency, besides reducing the inverter losses, mitigates the effects of dead-time harmonics [33]. For carrier-based techniques, the commutations are reduced when the modulating waveforms reach their limits, i.e., ± 1 p.u. [9]. On the other hand, for space-vector techniques, the switching frequency depends on the number of space vectors used in each sector and zone and their switching pattern [13]. In the following, the average switching frequency, normalized by the carrier frequency, is studied. It is computed by dividing the actual number of switching events

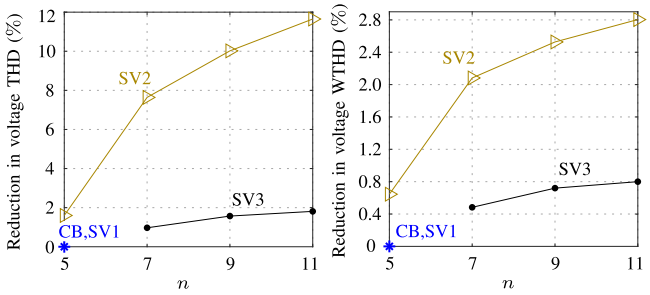

Fig. 10. Maximum reduction in voltage THD and voltage WTHD (current THD) by using the proposal instead of the existing methods versus n.

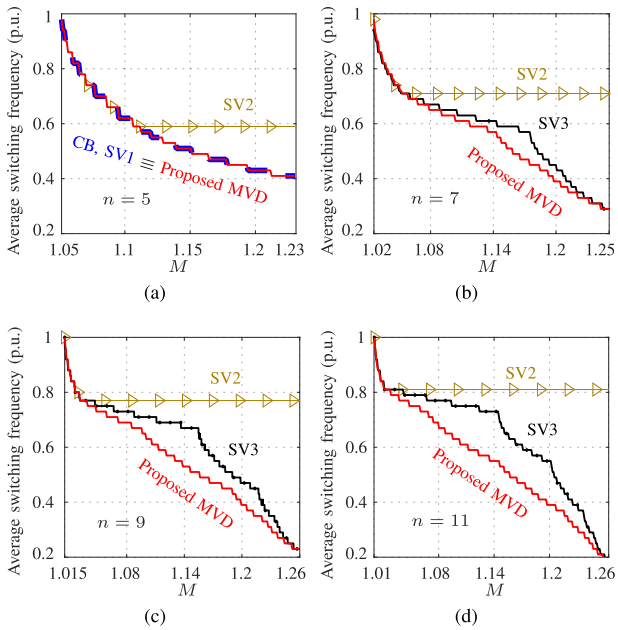

Fig. 11. Average switching frequency versus M for (a) $n = 5$, (b) $n = 7$, (c) $n = 9$, and (d) $n = 11$.

in one fundamental period by the number of switching events expected in the linear region of PWM, also in one fundamental period [19].

In general, the average switching frequency decays regardless of the method, as depicted in Fig. 11. In particular, that of SV2 diminishes for certain M at the beginning of the OVM range. However, for higher M, the switching frequency of SV2 stays constant and produces larger losses than SV3 and MVD for any n. For $n = 5$ in Fig. 11(a), the number of commutations of the proposal is exactly the same as for CB and SV1 and lower than for SV2. Nevertheless, for $n > 5$, it provides a significant advantage over SV2 and SV3. As shown in Fig. 11(b)–(d), the proposed MVD attains the smallest switching frequency for any M. Furthermore, this advantage is especially significant for $n > 5$. These features are also summarized in Table I.

C. Analysis of Computational Burden

The computational burden is evaluated by the methodology used in [7] and [16]. The Mathlib library for C66x DSP cores by Texas Instruments is used for determining the number of floating-point operations (flops) required by each calculation.

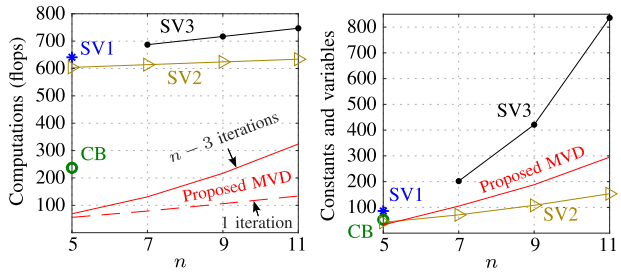

Fig. 12. Comparison of computational burden in terms of the maximum number of flops per sampling period and constants and variables prestored in memory.

One flop is needed for a comparison, assignment, real addition, subtraction, multiplication, or division. Moreover, operations such as the square root, four-quadrant arctangent atan2, sine, and cosine employ 89, 262, 101, and 108 flops, respectively. Furthermore, it is assumed that a sorting operation uses $n \log_2(n)$ flops by using the merge sorting method [7].

As depicted in Fig. 12, the proposed MVD needs many fewer flops than SV1, SV2, and SV3, and even less flops than CB. This feature of MVD is due to its lack of trigonometric functions and square roots and of intricate identification of sector/zones. Moreover, other computations, such as the inverse vector space decomposition as well as the min–max method used by CB, are no longer needed. Furthermore, taking advantage of the fact that a considerable number of constants in the $\boldsymbol{G_p}$ matrices are zero, many multiplications/additions are omitted. Concerning the iterative scheme of MVD, when just one iteration is required, the number of flops is marginal. Although the flops may increase to some extent with more iterations, in the worst case ($n - 3$ iterations), the proposed MVD needs much fewer flops than the existing strategies. Regarding memory resources, compared with previous techniques, the number of variables and constants prestored in the control platform for the proposed MVD is acceptable. SV2 employs fewer constants and variables, whereas SV3 needs substantial memory resources. The advantage of SV2 in terms of memory is of small relevance since it comes at the expense of a large current THD.

Accordingly, as listed in Table I, besides providing the minimum voltage THD as well as the smallest current THD and inverter witching losses, the proposal exhibits a low computational burden, especially in terms of flops. Indeed, the overall performance of the proposal is outstanding compared with space-vector methods, e.g., SV2 and SV3.

V. Experimental Results

Fig. 13 shows the test bench for the experimental validation. The drive consists of a symmetrical nine-phase four-pole induction motor. Notably, besides improved fault tolerance [1], [34], nine-phase motors are often preferred for industrial applications [34], because they can be easily obtained by rewinding standard three-phase frames [35] and can be fed by using off-the-shelf three three-phase inverters, as exploited here. The inverters are controlled by a dSPACE MicroLabBox platform. The motor is coupled to a dc generator, whose armature is connected to

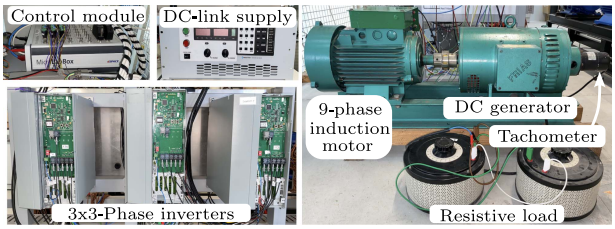

Fig. 13. Photographs of the experimental setup.

a resistive load. The rotor speed is measured by a tachometer. The inverters are driven with a switching (carrier) frequency of 10 kHz and dead time of 2 μs. Symmetrical regular-sampled PWM is used [29], where the modulating signal sampling is synchronized with the negative peaks. As in other papers [6], [7], [9], [16], [18], the voltage signals refer to those of the inverter voltage references to avoid harmonics due to inverter nonlinearities, electromagnetic noise, or aliasing, which do not affect the dc-link utilization. Each current signal is oversampled at 10 MHz and then averaged to remove high-frequency noise [6], [13], [18], [36], and afterward, a sample is taken at each negative peak of the carrier.

A. Motor Parameters

The nine-phase motor was obtained by rewinding the stator of a three-phase one. The double-layer windings of this nine-phase motor are close to sinusoidally distributed and are star connected with a single neutral point. The rated values of the voltage, current, speed, and frequency are 110 V, 2.2 A, 1430 r/min, and 50 Hz, respectively. The rated torque is 9.5 N $\cdot$ m and the peak torque is 15.2 N $\cdot$ m. The $\alpha\beta$ plane parameters are as follows: stator resistance of 3.6 Ω, rotor resistance of 8.5 Ω, magnetizing inductance of 430 mH, stator leakage inductance of 26.6 mH, and rotor leakage inductance of 23.3 mH.

Under the assumption of perfectly sinusoidal and balanced winding distribution, the impedances of all the xy planes are identical and given just by the same stator resistance (3.6 Ω) and stator leakage inductance (26.6 mH) as in the $\alpha\beta$ plane [3]. However, since sinusoidal distribution is difficult to achieve in practice [2], this assumption does not correctly reflect the behavior of the xy planes [18], [37], [38], [39]. Therefore, a more realistic model of these planes, as in [37], [38], and [39], is used here. It considers that the impedance of each xy plane has the same resistance, which is the stator resistance of 3.6 Ω, but a different stator leakage inductance per plane. By measuring the impedances, the inductances of the $(u_{x,1}, u_{y,1})$, $(u_{x,2}, u_{y,2})$, and $(u_{x,3}, u_{y,3})$ planes are found to be 26.6, 69.6, and 35.6 mH, respectively. In this model, the rotor parameters of the xy planes can be disregarded [38], [39]. Note that the machine model has no influence on the MVD method, since it does not depend on the motor parameters (see Section III-B), such as the stator leakage inductances of the xy planes, etc. This also holds for the previous techniques [5], [9], [12], [13] compared here.

In the following, the performance of MVD is validated by means of experiments in steady state (see Section V-B) and speed transients (see Section V-C). Steady-state experiments are performed under open-loop scalar V/f control, whereas experiments during transients are conducted under speed closed-loop scalar V/f control.

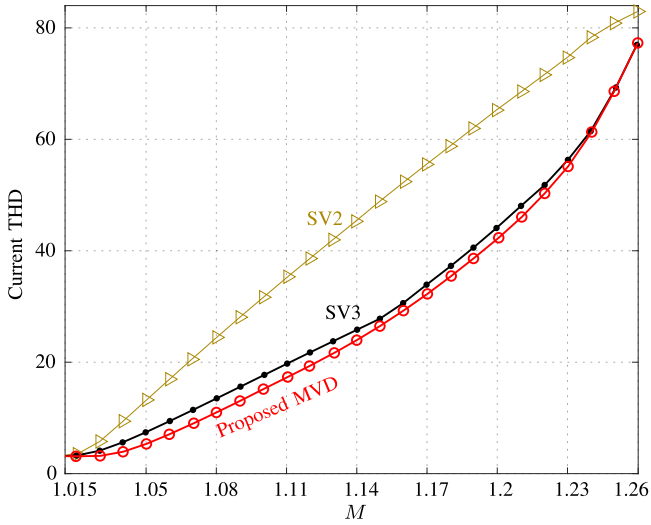

Fig. 14. Experimental current THD for the nine-phase induction motor.

B. Experiments in Steady State

The methods assessed in Section IV (those suitable for $n = 9$) are considered in this section. Moreover, the current THD and voltage THD are calculated based on the balanced harmonic orders below the Nyquist frequency (5 kHz) [18]. All the measurements are in steady state. As the motor load condition has negligible effects on the harmonic currents in OVM [15], the tests are performed without load to avoid overheating risk.

Similar to [6], [18], and [19], under open-loop scalar V/f control, the motor is driven up to its rated voltage and rated frequency. Then, the dc-link voltage $v_{\rm dc}$, initially equal to 306 V, is progressively decreased to 247 V. Besides providing a nearly constant air-gap flux [40] with a fundamental voltage amplitude of 110 V and a fundamental current amplitude of 0.83 A for any M, this procedure gives M values ranging from 1.015 up to 1.26, which cover the entire OVM range for $n = 9$ [11].

As shown in Fig. 14, the current THDs of SV2, SV3, and the proposal are in line with the voltage WTHD of Fig. 9(c). Although the absolute values differ due to the normalization by the fundamental current amplitude when computing the current THD, the relationships between the techniques are consistent with Fig. 9(c), which is of most importance. Thus, the theoretical assessments of Section IV-A are validated. Remarkably, the proposal attains the lowest current THD for every M, as predicted. Moreover, since the voltage references match those of the theoretical assessments, the voltage THDs of SV2, SV3, and the proposal equal those of Fig. 9(c), where the proposal achieves the minimum THD for any M.

Fig. 15 depicts the pole-voltage references, and currents of SV2, SV3, and MVD for $M = 1.10$ and $M = 1.13$ in Fig. 15(a) and (b), respectively. In accordance with the preceding remarks, the harmonic distortion in the voltages and currents of SV2 and SV3 is greater than those of the proposal. For example, for $M = 1.10$ in Fig. 15(a), the voltage THD is decreased from

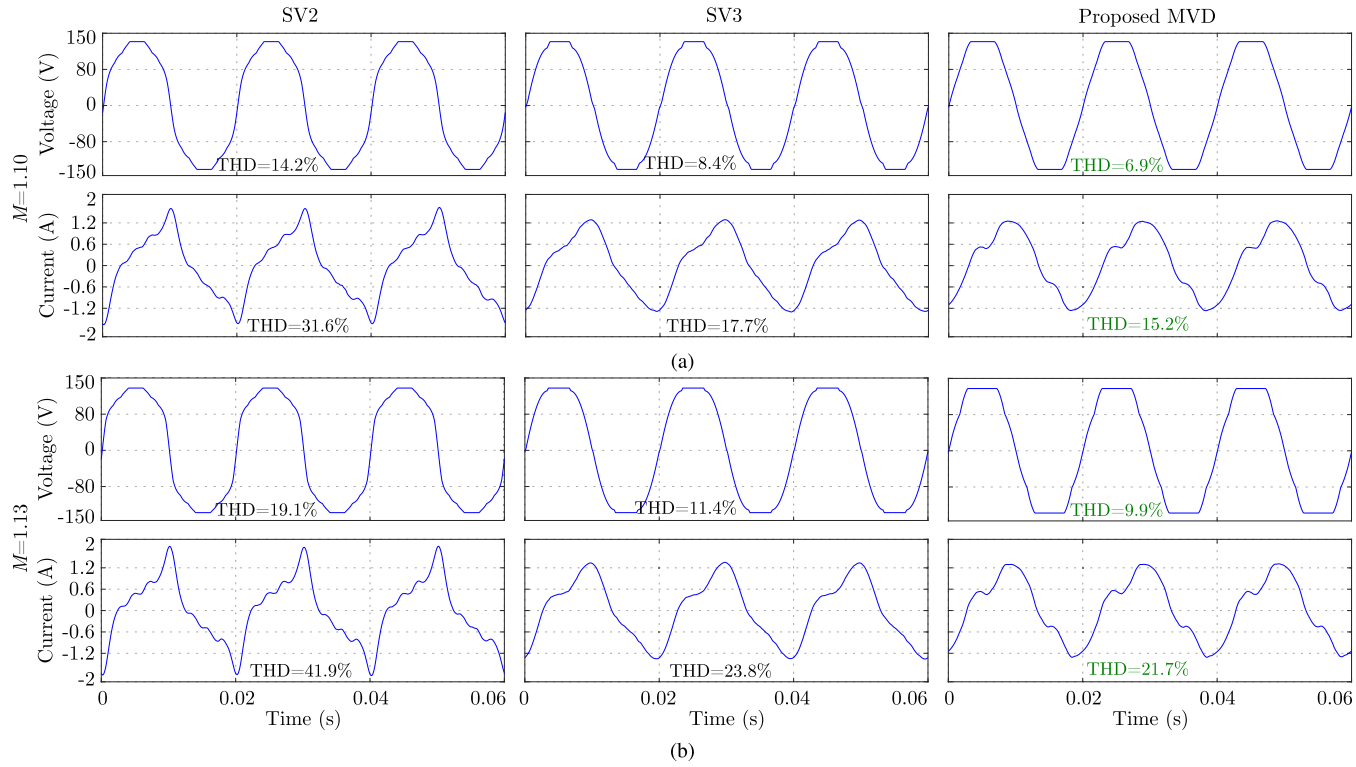

Fig. 15. Experimental waveforms of the voltage references and currents of phase a for (a) $M = 1.10$ and (b) $M = 1.13$.

TABLE II
CURRENT THD AND VOLTAGE THD FOR $M = 1.10, 1.13$

M	Voltage THD (%)			Current THD (%)		
	SV2	SV3	MVD	SV2	SV3	MVD
1.10	14.2	8.2	6.9	31.6	17.7	15.2
1.13	19.1	11.4	9.9	41.9	23.8	21.7

14.2% (SV2) or 8.4% (SV3) to 6.9% by employing the proposal. The reduction in terms of current THD is in line with that of the voltage THD. For said $M = 1.10$, the current THD decays from 31.6% (SV2) or 17.7% (SV3) to 15.2% by using the proposed MVD. These advantages of MVD over SV2 and SV3 are consistent not only for $M = 1.13$ in Fig. 15(b) but also for the entire OVM range (see Fig. 14). The THDs for $M = 1.10$ and $M = 1.13$ are summarized in Table II.

Fig. 16 shows the trajectories of the voltage references in each subspace, normalized by $0.5v_{\rm dc}$, for certain M values. The mapping of the harmonic orders per plane corresponds to that given in Section II-A. All the methods yield circular trajectories in the $\alpha\beta$ plane, avoiding torque ripple due to the injection of $\alpha\beta$ torque-producing harmonics. On the other hand, the harmonic content in the xy planes depends on the strategy. SV2 produces a notable harmonic distortion in each xy subspace for any M, as shown in Fig. 16(a). Concerning SV3, the harmonics are a function of M, as depicted in Fig. 16(b). For relatively low M, e.g., $M = 1.05$, $M = 1.10$, and $M = 1.15$, SV3 constrains the harmonic injection just to the $(v_{x,2}, v_{y,2})$ plane, containing mainly the third-order voltage harmonic. In contrast, the proposal diminishes this third-order harmonic by injecting instead higher order ones (with greater impedances) belonging to all xy planes [see Fig. 16(c)] so as to achieve the minimum voltage THD. This is beneficial since the third-order voltage harmonic is, in general, responsible for the largest current distortion in OVM [18]. Thus, said unnecessary constraint imposed by SV3 yields a suboptimal injection of xy voltages, which is more obvious for relatively low M. Eventually, as M rises, e.g., for $M = 1.20$ and $M = 1.23$, higher order harmonics from the remaining xy planes are added by SV3. Nevertheless, even in this scenario, the proposal is advantageous over SV3 (see Fig. 14). Note that, especially for relatively low M, e.g., for $M = 1.05$ or $M = 1.10$ in Fig. 16, the smallest $(v_{x,2}, v_{y,2})$ trajectories are for the proposal.

As aforesaid, a remarkable feature that stems from attaining the minimum voltage THD, as the proposal does, is leading to less current THD. Let us further investigate this fact by analyzing the voltage-reference and current spectra for, e.g., $M = 1.10$ and $M = 1.23$ in Figs. 17 and 18, respectively. From Fig. 17, SV3 injects only a third-order voltage harmonic, which sees a relatively low impedance and yields the largest current distortion. Although SV3 does not inject voltage harmonics of higher order than the third one for $M = 1.10$, some distortion appears in the fifth- and seventh-order current harmonics. This distortion, which also affects SV2 and the proposal, is caused by unavoidable nonideal effects such as dead time or flux-saturation [26], [41]. In contrast to SV3, the proposed MVD mitigates this third-order voltage-reference harmonic by injecting instead higher order ones, such as the fifth and seventh.

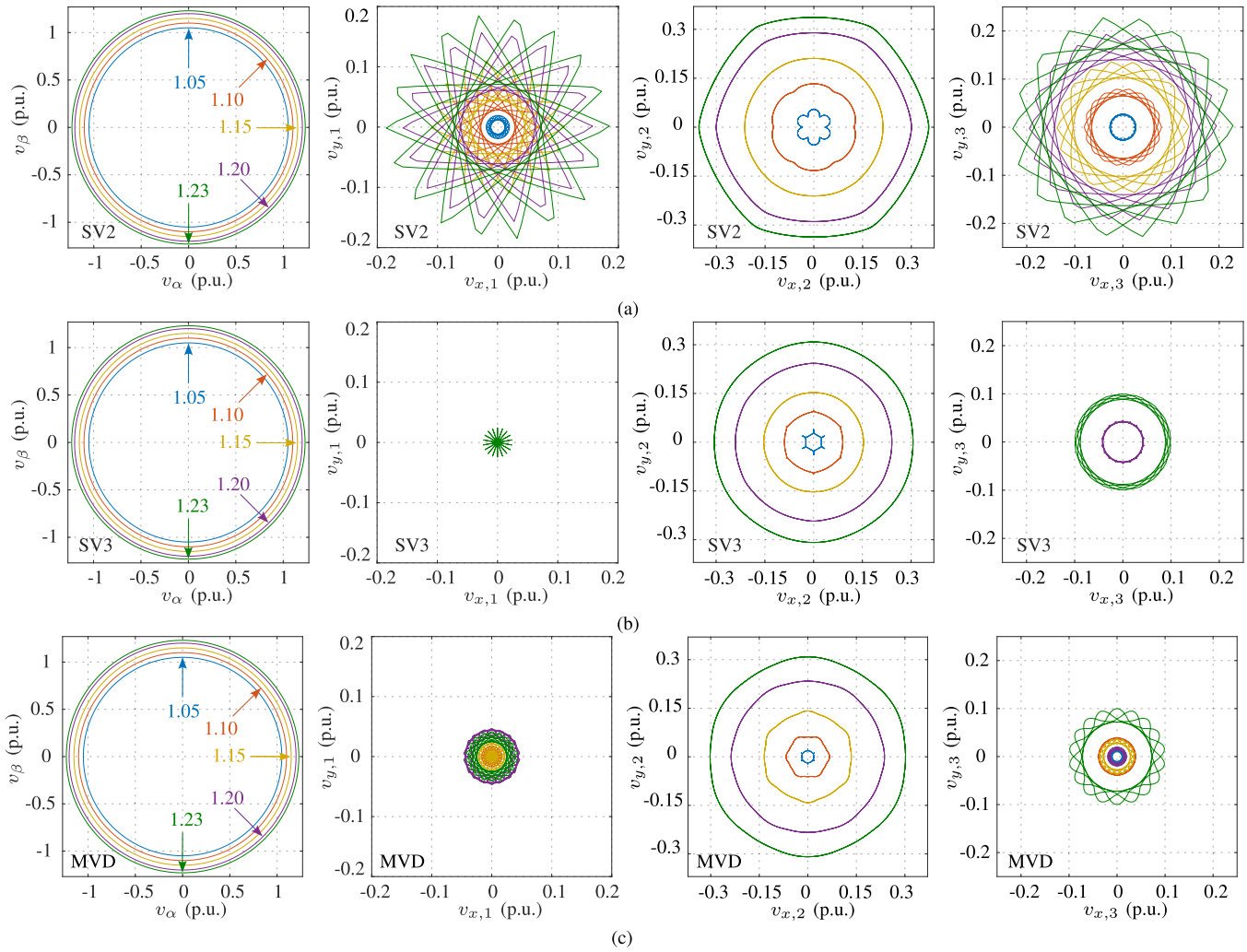

Fig. 16. Experimental loci of the voltage references, normalized by $0.5v_{\mathrm{dc}}$, for several values of M. (a) SV2. (b) SV3. (c) Proposal.

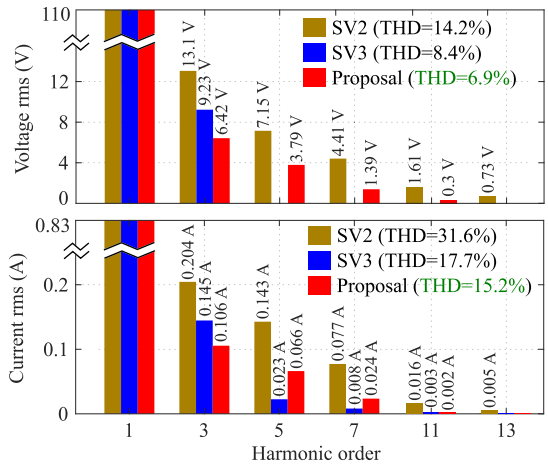

Fig. 17. Experimental voltage reference and current spectra for $M = 1.10$.

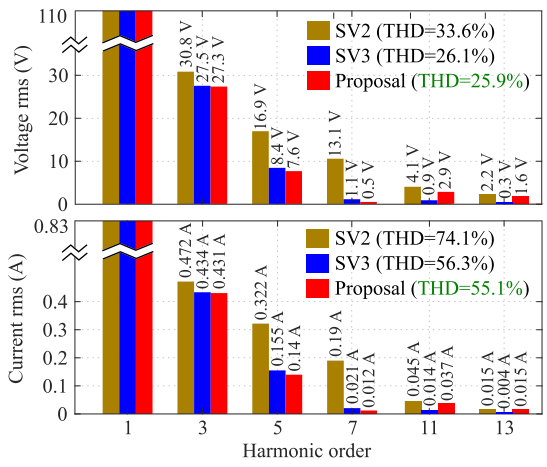

Fig. 18. Experimental voltage reference and current spectra for $M = 1.23$.

Although the impedances per harmonic are not considered in the optimization problem of MVD, the benefit of reducing the third-order harmonic is achieved thanks to the fact that MVD minimizes the voltage THD. Note that the lower order harmonics, especially the third and fifth, present a relatively larger impedance compared with those under the assumption of sinusoidally distributed windings. As discussed in Section V-A, this is mainly caused by the existence of certain parasitic space

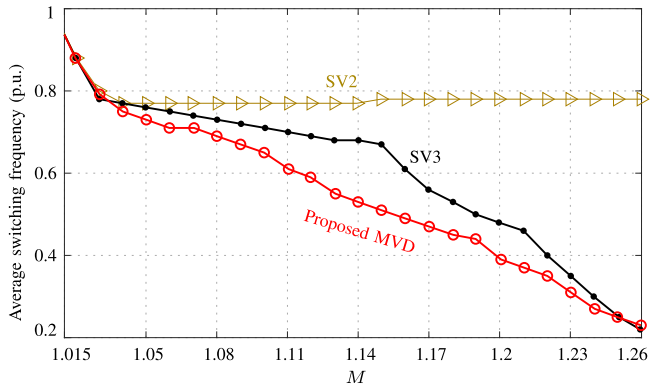

Fig. 19. Experimental inverter average switching frequency.

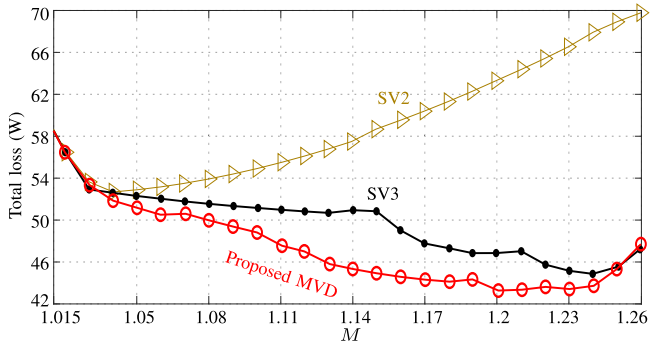

Fig. 20. Total loss, including stator copper loss plus inverter loss.

harmonics [42]. Thus, the currents are smaller than expected for these harmonics. Despite this fact, the proposed MVD is still advantageous in Fig. 17 over SV3 or SV2 by notably reducing the current THD. Therefore, the general validity of the main theoretical outcomes is corroborated, even for nonideal machines. For $M = 1.23$, depicted in Fig. 18, compared with the proposed MVD, SV3 now injects voltage harmonics of all xy planes. For this $M = 1.23$, the lower order voltage/current harmonics (third, fifth, and seventh) of SV3 are greater than for the proposed MVD. Hence, the proposal is also favorable even for high M.

Fig. 19 shows the average switching frequency for the OVM methods. As predicted in Fig. 11, for relatively low M, the switching frequency decays rapidly for all the techniques. However, for M above 1.05, the behavior diverges among the strategies. The switching frequency of SV2 remains nearly constant and is higher than for SV3 and the proposal. On the other hand, the commutations for SV3 and MVD drop as M rises. Conveniently, the proposed MVD yields a much lower switching frequency than SV3 for most M. This fact is consistent with Fig. 11(c), thus verifying the study of Section IV-B.

As already stated, reducing the current THD mitigates the stator copper loss and the inverter conduction losses [30], [31]. Similarly, lowering the switching frequency alleviates the switching losses [31], [43]. Accordingly, using the proposed MVD improves the drive efficiency compared with the existing techniques, as can be noticed in Fig. 20. It depicts the total loss, which is comprised of the stator copper loss and inverter loss. For a clear comparison, other losses, such as rotor, friction, or iron,

TABLE III
STATOR COPPER LOSS PLUS INVERTER LOSS FOR $M = 1.11, 1.15, 1.20$

M	Total loss (W)		
	SV2	SV3	MVD
1.11	55.5	51.0	47.5
1.15	58.8	50.8	44.9
1.20	63.3	47.1	43.4

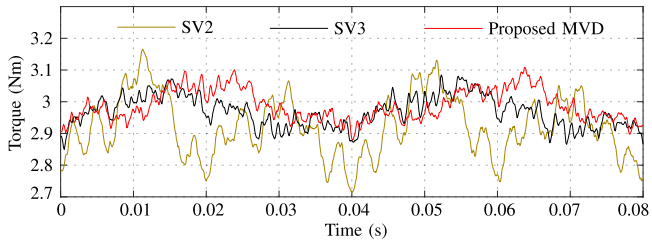

Fig. 21. Electromagnetic torque for $M = 1.10$.

are excluded from Fig. 20. In fact, these losses primarily depend on characteristics that are common for all techniques, such as fundamental flux (sinusoidal flux distribution is assumed), fundamental frequency, speed, etc. [31], [43], [44]. For computing the switching losses, the methodology in [43] is adopted. The parameters of the inverter module STGIPQ5C60T-HL are considered, whose ratings are comparable to those of the machine. Note that MVD is beneficial over existing techniques for almost every M (see Fig. 20). For example, for $M = 1.15$, the losses are reduced from 58.7 W (SV2) or 50.8 W (SV3) to 44.9 W by using MVD. Table III provides the losses, other than those for $M = 1.15$, for $M = 1.11$ and $M = 1.20$, where a noticeable advantage is obtained by MVD.

The electromagnetic torque for $M = 1.10$ is depicted in Fig. 21. It is estimated by using the measured currents and stator-flux observers as in [45]. Fig. 21 illustrates the torque for four fundamental periods and for $M = 1.10$. It can be noticed that some ripple appears for all methods, especially for SV2. These small oscillations, which also arise in the linear region of PWM, are principally caused by nonideal effects of the motor and the inverter [33], [42], not by distortion injected by the OVM methods. Actually, SV2, SV3, and MVD prevent the injection of torque-producing $\alpha\beta$ voltage harmonics by describing circular trajectories in the $\alpha\beta$ plane (see Fig. 16).

The study of Section IV-C is validated by measuring the execution times, which are depicted in Fig. 22. Regardless of the method, the V/f control, as well as other measurements, entails an extra run time of 12.7 μs apart from the times shown in Fig. 22. In agreement with Fig. 12, the proposed MVD shows an outstanding performance in Fig. 22, consuming just 1 μs when the maximum number of iterations/flops has been reached (for roughly $M \geq 1.24$). Even in this case, the execution time is at least five and six times less than for SV2 (5.5 μs) and SV3 (6.4 μs), respectively. For the latter methods, the run time is nearly constant. On the other hand, the execution time of the proposal decreases as M diminishes. Note that the particular $M = 1.015$ belongs to the boundary of the linear region of

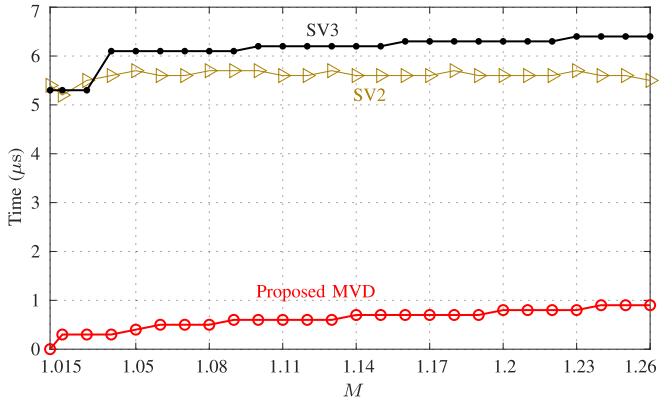

Fig. 22. Experimental execution time of the control platform.

TABLE IV
SUMMARY OF THE EXPERIMENTAL RESULTS

Method	Voltage THD	Current THD	Execution time	Switching frequency
SV2	High	High	Medium	High
SV3	Medium	Medium	High	Medium
Proposed MVD	Minimum	Low	Very low	Low

PWM and to the beginning of the OVM range. Thus, in this case, it is valid to apply either an OVM strategy or a suitable method for the linear region. The latter choice was applied for all techniques. For MVD, the measured execution time is almost zero since just min–max injection is performed. On the other hand, SV2 and SV3 yield a considerable run time. The reason is that, even for the linear region, these space-vector strategies need to perform several time-consuming tasks, such as sector identification, rotation of the $\alpha\beta$ space vector to the first sector, computing the dwell times of the active and zero space vectors, etc. [12], [13], [22]. The extra computational resources available by employing the proposal are useful for other critical tasks such as condition monitoring [7].

The main conclusions drawn from the experiments are listed in Table IV. They are consistent with the outcomes of the theoretical study of Section IV (see Table I). The performance of the proposal is advantageous in all the features studied.

C. Experiments in Transients

The performance of MVD is now assessed during speed transients. Moreover, a constant resistive load is now connected to the dc generator, enabling the motor to operate near its rated torque at rated rotor speed. To ensure that the motor follows the speed reference, a speed closed-loop scalar V/f control is implemented [46]. The proportional–integral speed control is designed as in [47]. The dc-link voltage is set to 250 V.

As can be seen in Fig. 23(a), the speed reference is changed stepwise at ≈ 0.03 s, from 1161 r/min up to the rated speed, i.e., 1430 r/min. As a result, M varies such that it spans almost the entire OVM range, from $M = 1.0$ (linear region of PWM) up to $M = 1.23$, as illustrated in Fig. 23(b). The voltage reference and current of phase a are shown in Fig. 23(c) and (d), respectively.

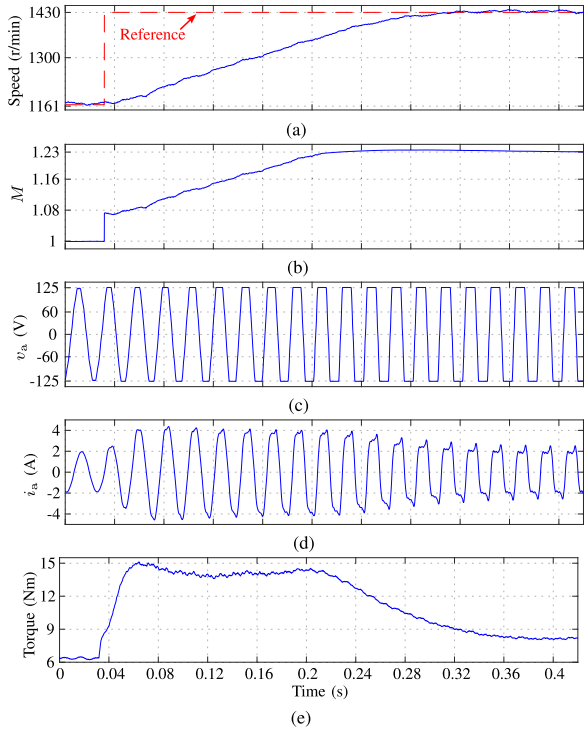

Fig. 23. Speed transient, with $v_{dc} = 250$ V. (a) Rotor speed. (b) M. (c) Voltage reference and (d) current of phase a. (e) Electromagnetic torque.

These signals change smoothly during the transient, and they reach their steady-state waveforms at ≈ 0.36 s, when rated speed and nearly rated electromagnetic torque are achieved. It can be noticed that the voltage reference exhibits a more square-like shape as M rises. The torque is depicted in Fig. 23(e). Prior to the reference change, the torque remains constant at 6 N · m. Subsequently, it rapidly increases to its peak value of 15.2 N · m immediately after the reference change, and then, it stabilizes at 8.2 N · m. Note that, in steady state, the torque is 6 N · m at 1161 r/min, while it is 8.2 N · m at 1430 r/min, as result of the speed dependence of the load torque. Most importantly, Fig. 23 proves that the performance of the proposed MVD in terms of torque and speed is satisfactory, even when their values are close to the rated ones.

From the experimental results, the proposed MVD is well suited for the normal operation of the drive, i.e., near rated speed and torque, in steady state or during transients.

VI. CONCLUSION

In this article, a carrier-based OVM method with minimum voltage THD for symmetrical induction motor drives with odd-n phases is proposed. To achieve the minimum voltage THD (i.e., the MVD), the proposal minimizes at each instant the xy content injected while reaching the requested modulation index. Unlike previous techniques based on this principle that were just for five phases, the proposal is suitable for any odd phase number.

Moreover, the existing techniques, including the proposal, are theoretically assessed for symmetrical machines with 5, 7, 9, and 11 phases. These studies provide valuable insight into the overall performance of OVM methods by considering the figures

of merit of voltage THD, current THD, switching frequency, and computational burden. To verify the theory, without loss of generality, the experiments have been performed with a symmetrical nine-phase induction motor with a single neutral point.

The main advantage of attaining the MVD in OVM is that the current THD is substantially mitigated, especially in machines with negligible space harmonics. Compared with the existing techniques, besides yielding the MVD for the first time, the proposal also achieves the smallest current THD for every modulation index. Interestingly, this advantage over previous methods becomes more significant as n rises.

Compared with previous techniques, the proposal also reaches the lowest average switching frequency. Hence, the switching losses are greatly alleviated. Actually, as a result of achieving the smallest current THD and the lowest switching frequency, the proposal attains the smallest stator copper losses and inverter losses, which improves the overall drive efficiency.

The proposal relies on carrier-based PWM. During the design, it is not necessary to perform tedious and intricate tasks as for most of the space-vector methods: vector mapping in each subspace, sector/zone identification, etc. Similarly, the online execution is much simpler.

Due to the benefits of MVD for OVM for symmetrical multiphase drives with odd n, future efforts should be aimed at extending the MVD method to asymmetrical drives, especially to dual three-phase drives. Moreover, the effectiveness of the proposal in permanent magnet synchronous motors should also be studied.

APPENDIX

The constants for $\boldsymbol{G}_p$ and $\boldsymbol{C}_p$ in (12) are

$$a_1 = 1.677; a_2 = -2.368; a_3 = 0.214; a_4 = 1.720;$$
$$a_5 = 0.406; a_6 = -0.657; a_7 = -1.618; a_8 = -4.045;$$
$$a_9 = -2.5; a_{10} = -1.314; a_{11} = -3.441; a_{12} = -4.236. \tag{A.1}$$

REFERENCES

[1] A. G. Yepes, O. Lopez, I. Gonzalez-Prieto, M. J. Duran, and J. Doval-Gandoy, "A comprehensive survey on fault tolerance in multiphase ac drives, Part 1: General overview considering multiple fault types," *Machines*, vol. 10, no. 3, 2022, Art. no. 208.

[2] E. Levi, "Multiphase electric machines for variable-speed applications," *IEEE Trans. Ind. Electron.*, vol. 55, no. 5, pp. 1893–1909, May 2008.

[3] E. Levi, R. Bojoi, F. Profumo, H. A. Toliyat, and S. Williamson, "Multiphase induction motor drives—A technology status review," *IET Electr. Power Appl.*, vol. 1, no. 4, pp. 489–516, 2007.

[4] W. N. W. A. Munim, M. J. Duran, H. S. Che, M. Bermúdez, I. González-Prieto, and N. A. Rahim, "A unified analysis of the fault tolerance capability in six-phase induction motor drives," *IEEE Trans. Power Electron.*, vol. 32, no. 10, pp. 7824–7836, Oct. 2017.

[5] G. Carrasco and C. Silva, "Space vector PWM method for five-phase two-level VSI with minimum harmonic injection in the overmodulation region," *IEEE Trans. Ind. Electron.*, vol. 60, no. 5, pp. 2042–2053, May 2013.

[6] A. G. Yepes and J. Doval-Gandoy, "Overmodulation method with adaptive x-y current limitation for five-phase induction motor drives," *IEEE Trans. Ind. Electron.*, vol. 69, no. 3, pp. 2240–2251, Mar. 2022.

[7] A. G. Yepes, J. Doval-Gandoy, and H. A. Toliyat, "Improvement in dc-link utilization with reduced current and torque deterioration for five-phase drives by combination of circulating-current filters and simple carrier-based PWM based on closed-form expressions," *IEEE Trans. Ind. Electron.*, vol. 68, no. 2, pp. 960–971, Feb. 2021.

[8] T. Komrska, T. Glasberger, and Z. Peroutka, "Universal PWM modulator for multiphase drives with a minimum infinity-norm approach," *IEEE Trans. Ind. Electron.*, vol. 63, no. 10, pp. 5979–5987, Jun. 2016.

[9] L. Vancini, M. Mengoni, G. Rizzoli, G. Sala, L. Zarri, and A. Tani, "Carrier-based PWM overmodulation strategies for five-phase inverters," *IEEE Trans. Power Electron.*, vol. 36, no. 6, pp. 6988–6999, Jun. 2021.

[10] E. Levi, D. Dujic, M. Jones, and G. Grandi, "Analytical determination of dc-bus utilization limits in multiphase VSI supplied ac drives," *IEEE Trans. Energy Convers.*, vol. 23, no. 2, pp. 433–443, Jun. 2008.

[11] S. Halasz, "Overmodulation region of multi-phase inverters," in *Proc. 13th Int. Power Electron. Motion Control Conf.*, 2008, pp. 682–689.

[12] J. Prieto, F. Barrero, M. J. Duran, S. Toral Marin, and M. A. Perales, "SVM procedure for n-phase VSI with low harmonic distortion in the overmodulation region," *IEEE Trans. Ind. Electron.*, vol. 61, no. 1, pp. 92–97, Jan. 2014.

[13] G. Yang et al., "Overmodulation strategy for seven-phase induction motors with optimum harmonic voltage injection based on sequential optimization scheme," *IEEE Trans. Power Electron.*, vol. 36, no. 12, pp. 14039–14050, Dec. 2021.

[14] M. J. Duran, J. Prieto, and F. Barrero, "Space vector PWM with reduced common-mode voltage for five-phase induction motor drives operating in overmodulation zone," *IEEE Trans. Power Electron.*, vol. 28, no. 8, pp. 4030–4040, Aug. 2013.

[15] C. Zhou, G. Yang, and J. Su, "PWM strategy with minimum harmonic distortion for dual three-phase permanent-magnet synchronous motor drives operating in the overmodulation region," *IEEE Trans. Power Electron.*, vol. 31, no. 2, pp. 1367–1380, Feb. 2016.

[16] A. G. Yepes and J. Doval-Gandoy, "Simple carrier-based PWM for prolonged high dc-link utilization for symmetrical and asymmetrical n-phase ac drives," *IEEE Trans. Power Electron.*, vol. 36, no. 8, pp. 8696–8712, Feb. 2021.

[17] A. Iqbal and E. Levi, "Space vector modulation schemes for a five-phase voltage source inverter," in *Proc. Eur. Conf. Power Electron. Appl.*, 2005, pp. 1–12.

[18] M. Medina-Sánchez, A. G. Yepes, O. López, and J. Doval-Gandoy, "Assessment and exploitation of the minimum current harmonic distortion under overmodulation in five-phase induction motor drives," *IEEE Trans. Power Electron.*, vol. 38, no. 4, pp. 4289–4305, Apr. 2023.

[19] S. Paul and K. Basu, "Overmodulation techniques of asymmetrical six-phase machine with optimum harmonic voltage injection," *IEEE Trans. Ind. Electron.*, vol. 68, no. 6, pp. 4679–4690, Jun. 2021.

[20] X. Zhang, T. Yang, and S. Bozhko, "Speed/torque ripple reduction of high-speed permanent magnet starters/generators with low inductance for more electric aircraft applications," *IEEE Trans. Transp. Electrific.*, vol. 8, no. 4, pp. 4431–4443, Dec. 2022.

[21] F. Bu, T. Pu, Q. Liu, B. Ma, M. Degano, and C. Gerada, "Four-degree-of-freedom overmodulation strategy for five-phase space vectorpulsewidth modulation," *IEEE J. Emerg. Sel. Topics Power Electron.*, vol. 9, no. 2, pp. 1578–1590, Apr. 2021.

[22] G. Yang, S. Li, H. Hussain, Z. Bai, and J. Yang, "Establishing optimized harmonic injection order of sequential overmodulation strategies for seven-phase induction motors," *IEEE Trans. Energy Convers.*, vol. 38, no. 1, pp. 739–742, Mar. 2023.

[23] A. Iqbal and S. Moinuddin, "Comprehensive relationship between carrier-based PWM and space vector PWM in a five-phase VSI," *IEEE Trans. Power Electron.*, vol. 24, no. 10, pp. 2379–2390, Oct. 2009.

[24] K. Zhou and D. Wang, "Relationship between space-vector modulation and three-phase carrier-based PWM: A comprehensive analysis [three-phase inverters]," *IEEE Trans. Ind. Electron.*, vol. 49, no. 1, pp. 186–196, Feb. 2002.

[25] M. Medina-Sánchez, A. G. Yepes, O. López, A. S. Abdel-Khalik, and J. Doval-Gandoy, "A carrier-based overmodulation strategy with minimum voltage distortion for symmetrical nine-phase induction motor drives," in *Proc. IEEE Energy Convers. Congr. Expo.*, 2023.

[26] A. G. Yepes, J. Malvar, A. Vidal, O. López, and J. Doval-Gandoy, "Current harmonics compensation based on multiresonant control in synchronous frames for symmetrical n-phase machines," *IEEE Trans. Ind. Electron.*, vol. 62, no. 5, pp. 2708–2720, May 2015.

[27] S. Boyd and L. Vanderberghe, *Convex Optimization*. Cambridge, U.K.:Cambridge Univ. Press, 2004.

[28] J. Sun, Z. Liu, Z. Zheng, and Y. Li, "An online global fault-tolerant control strategy for symmetrical multiphase machines with minimum losses in full torque production range," *IEEE Trans. Power Electron.*, vol. 35, no. 3, pp. 2819–2830, Jul. 2020.

[29] D. Holmes and T. Lipo, *Pulse Width Modulation for Power Converters*. Hoboken, NJ, USA: Wiley/IEEE Press, 2003.

[30] P. Stumpf and S. Halász, "Optimization of PWM for the overmodulation region of two-level inverters," *IEEE Trans. Ind. Appl.*, vol. 54, no. 4, pp. 3393–3404, Jul./Aug. 2018.
[31] H. Mahlfeld, T. Schuhmann, R. Döbler, and B. Cebulski, "Impact of overmodulation methods on inverter and machine losses in voltage-fed induction motor drives," in *Proc. 22nd Int. Conf. Elect. Mach.*, 2016, pp. 1064–1070.
[32] A. F. Abouzeid, J. M. Guerrero, A. Endemaño, I. Muniategui, D. Ortega, and F. Briz, "Assessment of overmodulation strategies for ac drives considering harmonics content and switching losses," in *Proc. IEEE Int. Electr. Mach. Drives Conf.*, 2021, pp. 1–6.
[33] S.-G. Jeong and M.-H. Park, "The analysis and compensation of dead-time effects in PWM inverters," *IEEE Trans. Ind. Electron.*, vol. 38, no. 2, pp. 108–114, Apr. 1991.
[34] R. R. Bastos, T. S. de Souza, M. M. de Carvalho, L. A. R. Silva, and B. J. C. Filho, "Assessment of a nine-phase induction motor drive for metal industry applications," *IEEE Trans. Ind. Appl.*, vol. 56, no. 6, pp. 7217–7226, Nov./Dec. 2020.
[35] A. S. Abdel-Khalik, A. Massoud, and S. Ahmed, "Standard three-phase stator frames for multiphase machines of prime-phase order: Optimal selection of slot/pole combination," *IEEE Access*, vol. 7, pp. 78239–78259, 2019.
[36] S. N. Vukosavic, L. S. Peric, and E. Levi, "Digital current controller with error-free feedback acquisition and active resistance," *IEEE Trans. Ind. Electron.*, vol. 65, no. 3, pp. 1980–1990, Mar. 2018.
[37] M. S. Abdel-Majeed et al., "Postfault operation of onboard integrated battery charger via a nine-phase EV-drive train," *IEEE Trans. Ind. Electron.*, vol. 68, no. 7, pp. 5626–5637, Jul. 2021.
[38] A. S. Abdel-Khalik, M. S. Abdel-Majeed, and S. Ahmed, "Effect of winding configuration on six-phase induction machine parameters and performance," *IEEE Access*, vol. 8, pp. 223009–223020, 2020.
[39] D. Hadiouche, H. Razik, and A. Rezzoug, "On the modeling and design of dual-stator windings to minimize circulating harmonic currents for VSI fed AC machines," *IEEE Trans. Ind. Appl.*, vol. 40, no. 2, pp. 506–515, Mar./Apr. 2004.
[40] K. Lee and Y. Han, "Reactive-power-based robust MTPA control for V/F scalar-controlled induction motor drives," *IEEE Trans. Ind. Electron.*, vol. 69, no. 1, pp. 169–178, Jan. 2022.
[41] M. Jones, S. N. Vukosavic, D. Dujic, and E. Levi, "A synchronous current control scheme for multiphase induction motor drives," *IEEE Trans. Energy Convers.*, vol. 24, no. 4, pp. 860–868, Dec. 2009.
[42] A. M. Shata, A. S. Abdel-Khalik, R. A. Hamdy, M. Z. Mostafa, and S. Ahmed, "Improved mathematical modeling of six phase induction machines based on fractional calculus," *IEEE Access*, vol. 9, pp. 53146–53155, 2021.
[43] J.-i. Itoh and T. Ogura, "Evaluation of total loss for an inverter and motor by applying modulation strategies," in *Proc. 14th Int. Power Electron. Motion Conf.*, 2010, pp. S12-21–S12-28.
[44] I. Boldea and S. A. Nasar, *The Induction Machines Design Handbook*. Boca Raton, FL, USA: CRC Press, 2010.
[45] C.-C. Wang and C.-H. Fang, "Sensorless scalar-controlled induction motor drives with modified flux observer," *IEEE Trans. Energy Convers.*, vol. 18, no. 2, pp. 181–186, Jun. 2003.
[46] M. Kazmierkowski, "Control of converter-fed induction motor drives,"in*The Industrial Electronics Handbook: Power Electronics and Motor Drives*. Boca Raton, FL, USA: CRC Press, 2011.
[47] L. Harnefors, S. E. Saarakkala, and M. Hinkkanen, "Speed control of electrical drives using classical control methods," *IEEE Trans. Ind. Appl.*, vol. 49, no. 2, pp. 889–898, Mar./Apr. 2013.

Martín Medina-Sánchez (Graduate Student Member, IEEE) received the M.Sc. degree in automation and control engineering from the Escuela Superior Politécnica de Chimborazo, Riobamba, Ecuador, in 2017. He is currently working toward the Ph.D. degree in electrical engineering with the Applied Power Electronics Technology Research Group, Universidade de Vigo, Vigo, Spain.

His research interests include multiphase drives and power electronics.

Alejandro G. Yepes (Senior Member, IEEE) received the M.Sc. and Ph.D. degrees in electrical engineering from the Universidade de Vigo, Vigo, Spain, in 2009 and 2011, respectively.

Since 2008, he has been working with the Applied Power Electronics Technology Research Group, Universidade de Vigo. From August 2016 to June 2018, he was a visiting Scholar with the Department of Electrical and Computer Engineering, Texas A&M University, College Station, TX, USA, after which he returned to the Universidade de Vigo. His research interests include ac power conversion, with special focus, currently, on multiphase drives.

Óscar López (Senior Member, IEEE) received the M.Sc. and Ph.D. degrees in electrical engineering from the University of Vigo, Vigo, Spain, in 2001 and 2009, respectively.

Since 2004, he has been an Assistant Professor with the University of Vigo, where he is currently a Member of the Applied Power Electronics Technology Research Group. His research interests include ac power switching converter technology.

Ayman Samy Abdel-Khalik (Senior Member, IEEE) received the Ph.D. degree in electrical engineering under a dual channel program between Alexandria University, Alexandria, Egypt, and Strathclyde University, Glasgow, U.K., in 2009.

He is currently a Professor with the Department of Electrical Engineering, Faculty of Engineering, Alexandria University. His current research interests include electrical machine design and modeling, electric drives, energy conversion, and renewable energy.

Dr. Abdel-Khalik is an Associate Editor for IEEE TRANSACTIONS ON INDUSTRIAL ELECTRONICS and an Editor-in-Chief for *Alexandria Engineering Journal*.

Jesús Doval-Gandoy (Member, IEEE) received the M.Sc. degree from the Polytechnic University of Madrid, Madrid, Spain, in 1991, and the Ph.D. degree from the Universidade de Vigo, Vigo, Spain, in 1999, both in electrical engineering.

He is currently a Professor and the Head of the Applied Power Electronics Technology Research Group, Universidade de Vigo. His research interests include ac power conversion.